Bacillus velezensis **HBXN2020 alleviates** ***Salmonella*** **Typhimurium-induced colitis by improving intestinal barrier integrity and reducing inflammation**

Linkang Wang,[1,2,3] Haiyan Wang,[1,2,3] Xinxin Li,[1,2,3] Mengyuan Zhu,[1,2,3] Dongyang Gao,[1,2,3] Dayue Hu,[1,2,3] Zhixuan Xiong,[1,2,3] Xiangmin Li[1,2,3]* and Ping Qian[1,2,3]*

[1]*National Key Laboratory of Agricultural Microbiology, Hubei Hongshan Laboratory, Huazhong Agricultural University, Wuhan, Hubei, 430070, People's Republic of China*.

[2]*College of Veterinary Medicine, Huazhong Agricultural University, Wuhan, Hubei, People's Republic of China*.

[3]*Key Laboratory of Preventive Veterinary Medicine in Hubei Province, the Cooperative Innovation Center for Sustainable Pig Production, Wuhan, Hubei, People's Republic of China*.

* Corresponding author: Ping Qian: Tel: 86-27-87282608; Fax: 86-27-87282608; E-mail: qianp@mail.hzau.edu.cn. Address: No. 1, Shizishan Street, Hongshan District, Wuhan City, Hubei Province, China.

* Co-corresponding author: Xiang-min Li: Tel: 86-27-87282608; Fax: 86-27-87282608; E-mail: lixiangmin@mail.hzau.edu.cn. Address: No. 1, Shizishan

Street, Hongshan District, Wuhan City, Hubei Province, China.

Abstract

Bacillus velezensis is a species of *Bacillus* that has been widely investigated because of its broad-spectrum antimicrobial activity. However, most studies on *Bacillus velezensis* have focused on the biocontrol of plant diseases, with few reports on antagonizing *Salmonella* Typhimurium infections. In this investigation, it was discovered that *Bacillus velezensis* HBXN2020, which was isolated from healthy black pigs, possessed strong anti-stress and broad-spectrum antibacterial activity. Importantly, *Bacillus velezensis* HBXN2020 did not cause any adverse side effects in mice when administered at various doses (1×10^7, 1×10^8, and 1×10^9 CFU) for 14 d. Supplementing *Bacillus velezensis* HBXN2020 spores, either as a curative or preventive measure, dramatically reduced the levels of *Salmonella* Typhimurium ATCC14028 in the mice's feces, ileum, cecum, and colon, as well as the disease activity index (DAI), in a model of colitis caused by this pathogen in mice. Additionally, supplementing *Bacillus velezensis* HBXN2020 spores significantly regulated cytokine levels (TNF-α, IL-1β, IL-6, and IL-10) and maintained the expression of tight junction proteins and mucin protein. Most importantly, adding *Bacillus velezensis* HBXN2020 spores to the colonic microbiota improved its homeostasis and increased the amount of beneficial bacteria (*Lactobacillus* and *Akkermansia*). All together, *Bacillus velezensis*

HBXN2020 can improve intestinal microbiota homeostasis and gut barrier integrity and reduce inflammation to help treat bacterial colitis.

Key words: *Bacillus velezensis*; antibacterial activity; *S.* Typhimurium-induced colitis; infections; gut health

Introduction

Salmonella Typhimurium (*S.* Typhimurium) is a major foodborne zoonotic pathogen that can cause diarrhea and colitis in humans and animals (Fabrega and Vila, 2013; Yang et al., 2021). According to reports, *Salmonella* infections are common in both industrialized and developing nations, posing a serious risk to public health and resulting in significant financial losses (Katiyo et al., 2019; Mohan et al., 2019). At present, antibiotics remain one of the most effective treatment strategies for *Salmonella* infections. However, numerous studies have reported that the prolonged use or misuse of antibiotics can lead to environmental pollution, an increase in multi-drug-resistant (MDR) bacteria, as well as gastrointestinal microbiota dysbiosis (Ferri et al., 2017; Paulson et al., 2015; Reyman et al., 2022). In order to tackle *Salmonella* infections, a hunt for novel antimicrobial drugs is now underway.

More research has recently demonstrated the critical role gut microbiota plays in reducing intestinal inflammation (Cristofori et al., 2021) and mending the intestinal barrier (Ohland and Macnaughton, 2010; Wang et al., 2020). The use of probiotics is a popular approach to modulating intestinal microbiota

nowadays. Among all probiotics, *Bacillus* is one of the most popular probiotic species because of its ability to form endospores that survive gastric transit, storage and delivery conditions (Gu et al., 2015). Furthermore, *Bacillus* species can generate extracellular enzymes and antimicrobial metabolites that inhibit enteric pathogens, which lowers the risk of infection and enhances nutrient utilization (Abdhul et al., 2015; Ouattara et al., 2017).

The recently identified *Bacillus velezensis* (*B. velezensis*) species of the *Bacillus* genus has a large capacity to generate a variety of secondary metabolites that possess broad-spectrum antibacterial activity (Ye et al., 2018). Previous studies have reported that *B. velezensis* exhibits varying degrees of probiotic effects on plants, livestock, poultry and fish. For instance, the combined use of *B. velezensis* SQR9 mutant and FZB42 improved root colonization and the production of secondary metabolites that are beneficial to cucumber (Shao et al., 2022). *B. velezensis* isolated from yaks was shown to enhance growth performance and ameliorate blood parameters related to inflammation and immunity in mice (Li et al., 2019). The dietary *B. velezensis* supplementation can regulate the innate immune response in the intestine of crucian carp and reduce the degree of intestinal inflammation damage induced by *A. veronii* (Zhang et al., 2019). Few studies have been conducted on the treatment or prevention of colitis caused by *S.* Typhimurium; instead, the majority of investigations on *B. velezensis* focused on the biocontrol of fungal infections in plants.

A strain of *B. velezensis* HBXN2020 with broad-spectrum antibacterial activity was selected from a vast number of *Bacillus* strains for this study. We aimed to investigate the effectiveness of *B. velezensis* HBXN2020 in alleviating *S.* Typhimurium-induced mouse colitis and assessed the biological safety of *B. velezensis* HBXN2020. Notably, *B. velezensis* HBXN2020 can alleviate symptoms and colon tissue damage in experimental colitis, as indicated by markers such as *S.* Typhimurium loads, TNF-α and ZO-1 levels. Moreover, *B. velezensis* HBXN2020 also increases the abundance of beneficial bacteria, specifically *Lactobacillus* and *Akkermansia*, within the colon microbiota. As a result, this research supports the creation of probiotic-based microbial products as a substitute method of preventing *Salmonella* infections.

Results

Genomic Characteristics

HBXN2020's complete genome was sequenced using the Illumina Hiseq and PacBio platforms. The results showed that HBXN2020 has a circular chromosome of 3,929,792 bp (Fig. 1A) with a GC content of 46.5%, including 3,744 protein-coding genes (CDS), 86 tRNA genes, and 27 rRNA genes (Table S1). Furthermore, the HBXN2020 genome also contains 13 different clusters of secondary metabolic synthesis genes. such as Fengycin (genomic position:1,865,856) and Difficidin (genomic position:2,270,091) (Table S2).

A phylogenetic tree based on genome-wide data from all 14 *Bacillus* strains demonstrated that the HBXN2020 belongs to the *B. velezensis* species (Fig. 1B). To further understand the classification status of HBXN2020, the online tool JSpeciesWS was used to calculate the average nucleotide identity (ANI) based on the BLAST (ANIb) method. As shown in Fig. S1, HBXN2020 was found to be a member of the *B. velezensis* species due to the high percentage of ANIb (more than 97%).

Growth curve and *in vitro* resistance against environmental assaults.

The growth of *B. velezensis* HBXN2020 was assessed in flat-bottomed 100-well microtiter plates by measuring the values of OD_{600} every hour using an automatic growth curve analyzer. After measurement, we found that *B. velezensis* HBXN2020 entered the logarithmic growth phase after 2 h, and reached a plateau after 10 h of culture (Fig. 2A).

Next, we evaluated the effect of physical, chemical, and biological sterilization conditions such as high temperature, strong acidity, and enzyme preparation on the survival of *B. velezensis* HBXN2020. The survival rate of *B. velezensis* HBXN2020 showed a decreasing trend with increasing temperature (Fig. 2B), but this decrease was not obvious. In a strong acid environment (pH 2.0), *B. velezensis* HBXN2020 maintained a high survival rate (Fig. 2C), suggesting that *B. velezensis* HBXN2020 spores can survive under extreme conditions. Based on these results, we hypothesized that *B.*

velezensis HBXN2020 spores might also exhibit improved survival in gastrointestinal tract environments. Therefore, we further evaluated the survival rate of *B. velezensis* HBXN2020 in bile salt (0.3%, v/v), simulated gastric fluid (pepsin 1 mg mL^{-1}, pH 1.2), and simulated intestinal fluid (trypsin 1 mg mL^{-1}, pH 6.8). As shown in Fig. 2D-F, *B. velezensis* HBXN2020 spores demonstrated significantly improved tolerance to these simulated gastrointestinal tract environments.

Antibiotic susceptibility of *B. velezensis* HBXN2020 and bacteriostasis effect *in vitro*.

In order to assess *B. velezensis* HBXN2020's drug resistance, 19 antibiotics that are frequently used in clinical settings were chosen. The results indicated that only polymyxin B had a relatively small inhibition zone diameter (less than 15 mm). Ampicillin, meropenem, minocycline, ofloxacin, and trimethoprim had the strongest inhibition on *B. velezensis* HBXN2020, with an inhibition zone diameter exceeding 30 mm (Fig. 3A). In addition, the experimental results showed that *B. velezensis* HBXN2020 was extremely sensitive to β-lactams, tetracyclines, and quinolone drugs. Then, we performed an inhibition test of *B. velezensis* HBXN2020 against seven common clinical pathogenic bacteria. The results showed that *B. velezensis* HBXN2020 had a similar inhibitory effect on standard and wild strains of *Escherichia coli* (*E. coli*), *Salmonella*, *Staphylococcus aureus* (*S. aureus*), and *Clostridium perfringens* (*C.*

perfringens), as well as wild strains of *Streptococcus suis* (*S. suis*), *Pasteurella multocida* (*P. multocida*), and *Actinobacillus pleuropneumoniae* (*A. pleuropneumoniae*). Except for the wild strains of *S. suis* and *A. pleuropneumoniae*, the diameter of the inhibition zone of other strains was above 15 mm (Fig. 3B, S2), while the size of the inhibition zone of *S. suis* and *A. pleuropneumoniae* was also more than 12 mm.

Biosafety evaluation of *B. velezensis* HBXN2020

We assessed the biological safety of *B. velezensis* HBXN2020 in a mouse model in order to ascertain its safety. After gavage with *B. velezensis* HBXN2020 spores for two weeks, we observed no significant difference in the body weight of each group of mice (Fig. 4A). The gene expression levels of TNF-α, IL-1β, IL-6, and IL-10 of colon from all groups of mice exhibited no remarkable changes (Fig. 4B). However, in the colon, mRNA levels of the barrier proteins ZO-1 and occludin were trending towards an increase compared with the control group (Fig. 4C). Additionally, blood routine tests and serum biochemistry tests were performed for mice in the control group and H-HBXN2020 group on the 14th d after oral administration of *B. velezensis* HBXN2020 spores multiple times. As shown in Fig. 4D and S3, the blood parameters of mice after *B. velezensis* HBXN2020 treatment, including red blood cells (RBC), mean corpuscular volume (MCV), mean corpuscular hemoglobin (MCH), hemoglobin (HGB), white blood cells (WBC), platelets

(PLT), hematocrit (HCT), and mean corpuscular hemoglobin concentration (MCHC), were consistent with those of healthy mice. The serum biochemical parameters, including alanine aminotransferase (ALT), aspartate aminotransferase (AST), albumin (ALB), total bilirubin (TBIL), serum creatinine (CREA), and blood urea nitrogen (BUN), were also within normal limits (Fig. 4E). The corresponding histological analysis of colon tissue from mice receiving low, medium, and high doses of *B. velezensis* HBXN2020 spores (L-HBXN2020, M-HBXN2020, and H-HBXN2020 groups, respectively) is presented in Fig. 4F. The colon tissue sections of mice in the test groups showed no significant differences compared to the control group. Additionally, there were no observable differences in the major organ tissues (heart, liver, spleen, lung, and kidney) of mice treated with the high dose of *B. velezensis* HBXN2020 spores compared to healthy mice (Fig. S4). The results of this trial show that *B. velezensis* HBXN2020 is safe to use and has no negative side effects in mice.

Oral administration of *B. velezensis* HBXN2020 spores alleviated *S.* Typhimurium-induced colitis.

Testing both solid and liquid co-culture methods to see if *B. velezensis* HBXN2020 might suppress *S.* Typhimurium ATCC14028 (STm), the findings indicated that *B. velezensis* HBXN2020 decreased the development of STm in a dose-dependent manner (Fig. 5A, S5). Next, the therapeutic potential of *B.*

velezensis HBXN2020 was evaluated in an STm-induced mouse colitis model. At days 1, 3, and 5 after STm infection, mice in the STm + HBXN2020 group were orally administered *B. velezensis* HBXN2020 spores by gavage (Fig. 5B), while the control group and STm + PBS group were treated with sterile PBS. Also, the number of excreted STm in feces was counted daily at the designated time points. As shown in Fig. 5C, there was a significant and continuous reduction in the number of STm in feces following treatment with *B. velezensis* HBXN2020 spores, while the number of *B. velezensis* HBXN2020 viable bacteria in feces is also gradually decreasing (Fig. S6A). The number of STm in mouse feces was reduced by 10 to 50 times compared to the STm + PBS group from day 2 to 7 post-treatment. *B. velezensis* HBXN2020 spore treatment also resulted in a 5 to 10-fold reduction in the number of STm in the ileum, cecum, and colon, respectively (Fig. 5D-F). The increased inhibition of STm after *B. velezensis* HBXN2020 spore treatment also resulted in less weight loss and a marked reduction ($P < 0.001$) in DAI scores in STm + HBXN2020 group mice (Fig. 5G-H). In addition, we also measured the colon length of the mice and found that the STm + PBS group had a significantly shorter colon length ($P < 0.001$) than the control group. However, compared to the STm + PBS group, the STm + HBXN2020 group exhibited a longer colon ($P < 0.05$) (Fig. 5I-J).

To further assess the impact of *B. velezensis* HBXN2020 on the intestinal tract, we histologically analyzed their colonic tissues. The results showed that

mice treated with *B. velezensis* HBXN2020 spores exhibited a lower histology score (total scoring) ($P < 0.05$) (Fig. 6A, S6B) than mice not treated with the spores and were similar to that of healthy mice (control group). The colon tissue of mice not treated with *B. velezensis* HBXN2020 spores displayed higher histological scores, with significant crypt deformation, severe mucosal damage, and obvious inflammatory cell infiltration. These findings suggested that *B. velezensis* HBXN2020 can alleviate colon tissue damage. Moreover, we measured the mRNA levels of inflammatory cytokines, including tumor necrosis factor-α (TNF- α), interleukin-1 β (IL-1 β), interleukin-6 (IL-6), and interleukin-10 (IL-10) in colon tissue using RT-qPCR analysis. As shown in Fig. 6B-D, the mRNA levels of TNF-α ($P < 0.01$), IL-1β ($P < 0.05$), and IL-6 ($P < 0.05$) in the colon tissue of STm-infected mice were significantly upregulated, indicating the successful establishment of the STm-induced colitis model. As expected, treatment with *B. velezensis* HBXN2020 spores led to a significant reduction in the mRNA levels of these pro-inflammatory cytokines, while the mRNA levels of the anti-inflammatory cytokine IL-10 were significantly increased ($P < 0.01$) (Fig. 6E), suggesting that *B. velezensis* HBXN2020 spores can alleviate the inflammatory reaction of the colon. Moreover, the mRNA expression levels of colonic epithelial barrier proteins, including ZO-1, ocludin, claudin, and Muc2, were also measured by RT-qPCR. Compared with the PBS-treated group, the *B. velezensis* HBXN2020 spores treatment group exhibited significantly upregulated mRNA expression levels of ZO-1 (*P*

< 0.05), occludin (P < 0.05), claudin (P < 0.05), and Muc2 (P < 0.01) in the colon tissue (Fig. 6F-I), further demonstrating the ability of *B. velezensis* HBXN2020 to reduce damage to the colon epithelial barrier.

Next, we used 16S rRNA gene sequencing to investigate the impact of HBXN2020 spores on the makeup of the intestinal microbiota in mice treated with STm. The alpha diversity of colonic microbiota was evaluated using Sobs, Chao1, Shannon, and Simpson indices (OTU levels). Compared with the control and HBXN2020 group, the Sobs, Chao1, and Shannon indices of the STm + PBS group clearly decreased (Fig. 7A-C), while the Simpson index significantly increased (P < 0.05, Fig. 7D). Principle component analysis (PCA) based on Bray-Curtis distance showed that compared with the STm + PBS group, the gut microbiota composition of the STm + HBXN2020 group and the control group were more closer together (R=0.3988, P=0.001, Fig. 7E). We analyzed the community composition of colonic microbiota at the phylum and genus level, and the results revealed that the composition of the gut microbiota changed markedly after STm-induced mice. At the phylum level, the STm + PBS group increased the abundance of *Verrucomicrobiota* and *Proteobacteria* and decreased the abundance of *Firmicutes*, *Patescibacteria*, *Desulfobacterota*, and *Actinobacteriota* compared to the Control group (Fig. 7F). The HBXN2020 group increased the abundance of *Bacteroidota* and *Firmicutes* and decreased the abundance of *Verrucomicrobiota* compared with the Control group. On the contrary, the relative abundance of *Firmicutes*,

Patescibacteria, *Desulfobacterota*, and *Actinobacteriota* in the STm + HBXN2020 group was significantly higher than that in the STm + PBS group. At the genus level, infection with *S.* Typhimurium ATCC14028 in the STm + PBS group dramatically reduced the relative abundance of *norank_f_Muribaculaceae*, *Desulfovibrio* and *Lactobacillus* (Fig. 7G, H-I) and enhanced the abundance of *Bacteroides*, *Escherichia-Shigella*, *Salmonella*, *Alistipes*, and *Enterococcus* compared to the Control group (Fig. 7G, J-K). The HBXN2020 group increased the abundance of *norank_f_Muribaculaceae* and *Alloprevotella* compared to the Control group. In contrast, the STm + HBXN2020 group significantly improved the relative abundance of *norank_f_Muribaculaceae* and *Lactobacillus* compared with the STm + PBS group ($P < 0.01$, $P < 0.001$, Fig. 7H-I). In addition, LEfSe analysis was also performed to identify specialized microbial communities between the STm + HBXN2020 group and the STm + PBS group and found that there was a clear difference in gut microbiota composition between them. The microbiota that played a major role in the STm + PBS group were harmful *Enterobacterales* (Fig. 7L), while the STm + HBXN2020 group was *Candidatus_Saccharimonas*.

Prophylactic *B. velezensis* HBXN2020 spores alleviated *S*. Typhimurium-induced colitis.

Based on the improved therapeutic efficacy of *B. velezensis* HBXN2020 in the treatment of STm-induced colitis in mice, we further explored its potential

for disease prevention by evaluating pretreatment. Mice in the PBS + STm group and HBXN2020 + STm group were given the same amount of sterile PBS and *B. velezensis* HBXN2020 spores by gavage one week in advance. As shown in Fig. 8, compared with the PBS + STm group, oral administration of *B. velezensis* HBXN2020 spores as a preventive measure remarkably alleviated STm-induced colitis, including weight loss of mice ($P < 0.01$) (Fig. 8B), a significant reduction in DAI ($P < 0.001$) (the comprehensive score of weight loss, stool consistency, and blood in the feces, Fig. 8C), and the prevention of colon length shortening (Fig. 8D-E). However, the number of *B. velezensis* HBXN2020 viable bacteria in feces is also gradually decreasing with time prolonging (Fig. S8A). Furthermore, compared with the PBS + STm group, oral administration of *B. velezensis* HBXN2020 spores not only reduced the number of STm in mouse feces (Fig. 8F) but also decreased STm colonization in the ileum, cecum, and colon (Fig. 8G-H, S8B).

Histological analysis further revealed that oral administration of *B. velezensis* HBXN2020 significantly reduced the infiltration of inflammatory cells, mucosal damage and the overall histological score of colon tissue (Fig. 9A, S8C). Additionally, the mRNA expression levels of proinflammatory cytokines, including TNF-α ($P < 0.05$), IL-1β ($P < 0.05$) and IL-6 ($P < 0.01$), in the colon tissue of mice pretreated with *B. velezensis* HBXN2020 spores were significantly decreased (Fig. 9B-D), while the mRNA levels of anti-inflammatory cytokine (IL-10) were significantly higher ($P < 0.05$) (Fig. 9E)

than mice pretreated with PBS. In addition, compared to the group pretreated with PBS, the group pretreated with *B. velezensis* HBXN2020 spores showed a significant increase in mRNA expression levels of ZO-1 ($P < 0.001$), occludin ($P < 0.05$) and claudin ($P < 0.05$) in the colon tissue of mice (Fig. 9F-H). While there was no significant difference in Muc2 expression (p=0.252) (Fig. 9I), the results were consistent with those of the therapeutic experiments. Overall, these findings suggest that *B. velezensis* HBXN2020 can effectively alleviate the symptoms of STm-induced colitis and the associated damage to colon tissue.

Next, we examined the impact of prophylactic *B. velezensis* HBXN2020 on the intestinal microbiota composition of STm-treated mice. Sobs, Chao1 index and Shannon index have changed to some extent between groups, but differences were not significant (Fig. 10A-C). Compared with the Control group, the Simpson index significantly decreased in the PBS + STm group ($P < 0.05$, Fig. 10D). However, compared to the PBS + STm group, Simpson index in the HBXN2020 + STm group did not change (Fig. 10D). PCA analysis showed significant separation between control and PBS + STm groups, while the HBXN2020 + STm group, HBXN2020 group, and the control group were clustered together (Fig. 10E). Next, we analyzed microbial community composition at the phylum and genus levels. At the phylum level, the PBS + STm group increased the abundance of *Bacteroidota*, *Proteobacteria*, *Actinobacteriota*, and *Deferribacterota* and reduced the abundance of

Verrucomicrobiota, *Firmicutes*, *Patescibacteria*, and *Desulfobacterota* compared with the Control group (Fig. 10F). The HBXN2020 group increased the abundance of *Bacteroidota* compared to the control group. In contrast, compared to the PBS + STm group, the abundance of *Firmicutes* in the HBXN2020+STm group was significantly increased ($P < 0.05$). At the genus level, a depletion of *Lactobacillus* and *Akkermansia* (Fig. 10G, H-I) and an enrichment of *Alistipes*, *Bacteroides*, *Escherichia-Shigella*, *Alloprevotella*, *Helicobacter*, *Enterococcus*, and *Salmonella* were observed in PBS + STm group compared with the control (Fig. 10G, J-M). The enrichment with *norank_f_Muribaculaceae* and *Alloprevotella* was observed in the HBXN2020 group compared to the control. In contrast, an enrichment of *Lactobacillus*, *Akkermansia*, and *Lachnospiraceae_NK4A136_group* and a sharp decrease of *Alistipes*, *Bacteroides*, *Escherichia-Shigella*, *Salmonella*, and *Enterococcus* were observed in HBXN2020 + STm group compared to the PBS + STm group. LEfSe analysis showed that the abundance of *Lactobacillus* in the intestinal microbiota of mice was significantly increased after *B. velezensis* HBXN2020 treatment, while the abundance of harmful *Enterobacterales* in the untreated group was clearly increased (Fig. 10N).

Discussion

S. Typhimurium is an important intestinal pathogen that can cause invasive intestinal diseases such as bacterial colitis (Herp et al., 2019; Schultz et al.,

2017). Antibiotics are frequently used to treat colitis caused by bacteria; nevertheless, in recent years, their abuse has greatly increased bacterial resistance, leading to serious environmental pollution. A recent study showed that antibiotic-resistance genes in probiotics could be transmitted to the intestinal microbiota, which may threaten human health (Crits-Christoph et al., 2022). It is crucial to consider the source of probiotics. Strong environmental adaptability and disease resistance make black pigs an outstanding household breed in China (Yang et al., 2022). In this study, *B. velezensis* HBXN2020 was isolated from the free-range feces of black piglets in a mountain village in Xianning City (Hubei, China) and exhibited excellent antibacterial activity. Otherwise, *in vitro* tolerance assays showed that *B. velezensis* HBXN2020 spores have good tolerance to high temperature, strong acids, bile salts, as well as simulated gastric and intestinal fluid, which was similar to previous research results (Du et al., 2022). Furthermore, studies for antibiotic susceptibility revealed that *B. velezensis* HBXN2020 is not resistant to antibiotics.

Probiotics are distinct from food or medications in that they can cause toxins or infections in the body when ingested, and they are living when swallowed (Sanders et al., 2010; Snydman, 2008). Therefore, assessing the biosafety of probiotics is crucial. In this study, the safety of *B. velezensis* HBXN2020 was evaluated by measuring the body weight, intestinal barrier proteins, and inflammatory cytokines of the experimented mice, as well as

conducting routine blood and biochemical tests. The results showed that the expression levels of ZO-1 and occludin in the colon of mice increased after treatment with different doses of *B. velezensis* HBXN2020 spores. It has been reported that ZO-1, occludin and claudin are the three most important tight junction proteins in intercellular connections, which play a crucial role in maintaining the intestinal epithelial barrier (Bazzoni et al., 2000; Zihni et al., 2016). Thus, it is possible to improve intestinal barrier function by upregulating ZO-1 and occludin expression levels.

Important aminotransferases in animals, aspartate aminotransferase (AST) and alanine aminotransferase (ALT), are regarded as critical metrics for assessing liver function damage (Gou et al., 2022; Ozer et al., 2008). Under normal circumstances, the levels of ALT and AST are in dynamic balance without notable changes. However, when the liver is damaged or becomes dysfunctional, the levels of aminotransferases (ALT and AST) increase significantly (Tang et al., 2012). Previous studies have shown that CCL4-induced liver injury strongly increases plasma ALT/AST levels (Singhal et al., 2018). Zhang et al. reported that the addition of *Bacillus subtilis* to chicken diets significantly decreased the serum levels of ALT and AST (Zhang et al., 2017). In this present study, the levels of ALT and AST in the probiotic-treated group were slightly lower than those in the control group, indicating that *B. velezensis* HBXN2020 had no negative effect on liver health in mice. The *B. velezensis* HBXN2020 treatment group's blood indices were also found to be

comparable to those of the control group, falling within the normal reference range, according to regular blood testing.

Mice were fed with *B. velezensis* HBXN2020 spores orally after being challenged with *S.* Typhimurium ATCC14028 in order to assess the spores' potential to alleviate colitis caused by S. Typhimurium. Our experimental results demonstrated that oral treatment with *B. velezensis* HBXN2020 spores could alleviate *S.* Typhimurium-induced colitis, as evidenced by decreased weight loss, DAI, and histological damage, which is similar to prior studies (Cao et al., 2019; Wu et al., 2022). Previous research showed that macrophages are the first line of host defense against bacterial infection. They release proinflammatory cytokines, which are critical in initiating adaptive immune responses (Cheng et al., 2014; Dinarello, 2000). Nevertheless, proinflammatory cytokines have immunological properties that can be beneficial for the host to resist the invasion of bacteria and other microbes in the surrounding environment (Liu et al., 2021). For instance, pretreatment with recombinant murine TNF-α was shown to protect mice against lethal bacterial (*E. coli*) infection (Cross et al., 1989). PJ-34 exerted protective effects on intestinal epithelial cells against invasive *Salmonella* infection by upregulating IL-6 expression through the ERK and NF-κB signal pathways (Huang, 2009).

On the other hand, some research has demonstrated that over-activation of immune cells can result in tissue damage, organ failure, systemic or

persistent inflammation, and autoimmune diseases (Karki et al., 2021; Kotas and Medzhitov, 2015). IL-10 is a recognized anti-inflammatory mediator that plays a crucial role in maintaining intestinal microbe-immune homeostasis, regulating the release of inflammatory mediators, and inhibiting proinflammatory responses of innate and adaptive immunity (Maloy and Powrie, 2011; Ouyang et al., 2011; Saraiva et al., 2020). For instance, previous studies have shown that *Clostridium butyrate* can induce the production of IL-10 in the intestine, thereby alleviating experimental colitis in mice (Hayashi et al., 2013). Similar results were observed in our study, where oral administration of *B. velezensis* HBXN2020 spores reduced the expression levels of TNF-α, IL-1β, and IL-6 while increasing the levels of IL-10 in the colon of mice. Additionally, as demonstrated by the decreased histological damage and increased expression levels of intestinal barrier proteins, oral treatment of *B. velezensis* HBXN2020 spores reduced the functional damage of the intestinal barrier induced by S. Typhimurium infection.

Subsequently, we conducted additional analysis on the colon microbiome. Notably, oral *B. velezensis* HBXN2020 significantly raised the colonic microbiota's alpha diversity. As reported in prior studies, elevated alpha diversity is associated with enhanced anti-interference ability (Chen et al., 2021). PCA analysis results showed that oral administration of *B. velezensis* HBXN2020 significantly affected the structure of the intestinal microbiota.

Further analysis at the phylum/genus level revealed that *B. velezensis* HBXN2020 treatment reduced the increase of *Bacteroides*, *Escherichia-Shigella*, and *Salmonella* (harmful to intestinal homeostasis) in colitis (Wang et al., 2023) but enhanced the relative abundance of *Lactobacillus* (known for enhancing the epithelial barrier by increasing mucus secretion and upregulating the expression of tight junction proteins such as claudin-1, occludin, and ZO-1) (Kaur et al., 2021) and *Akkermansia* (known for modulating intestinal immune response by producing short chain fatty acids and reducing the secretion of proinflammatory cytokines) (Cani et al., 2022). *Bacteroides* are generally 'friendly' commensals in the intestine, but they can enter normal tissues through the intestinal mucosa when intestinal barrier function becomes compromised (Polk and Kasper, 1977), leading to inflammation, diarrhea, and abdominal abscesses (Pickard et al., 2017). *Escherichia-Shigella* is a common intestinal pathogen, and its relative abundance is associated with proinflammatory states (Morgan, 2013). *Salmonella* can secrete bacterial virulence proteins, which are directly delivered to the host cell cytosol through the Type III secretion system and induce the expression of pro-inflammatory cytokines (Hardt et al., 1998), leading to inflammation. Overall, the *S*. Typhimurium ATCC14028 infection altered the structure of the colon microbiota and raised the relative abundance of pathogenic bacteria, whereas the therapeutic *B. velezensis* HBXN2020 increased the abundance of beneficial bacteria, decreased inflammation, and

enhanced the function of the intestinal barrier.

We assessed pretreatment in order to learn more about the potential of *B. velezensis* HBXN2020 spores for disease prevention, given the increased efficacy of treating colitis caused by S. Typhimurium. Similarly to the therapeutic effect of oral *B. velezensis* HBXN2020, pretreatment with *B. velezensis* HBXN2020 spores effectively alleviated the symptoms of *S.* Typhimurium-induced colitis and reduced the expression levels of proinflammatory cytokines and increased anti-inflammatory cytokine levels in the colon of *S.* Typhimurium-infected mice. Furthermore, pretreatment with *B. velezensis* HBXN2020 spores also promoted the expression levels of intestinal barrier proteins in the colon of *S.* Typhimurium-infected mice. In addition, the microbiota composition was also dramatically modulated by prophylactic *B. velezensis* HBXN2020 in mice with colitis, although the community richness and diversity revealed by the alpha diversity index were not significantly impacted in mice with colitis by prophylactic treatment. Prophylactic *B. velezensis* HBXN2020 significantly boosted SCFA-producing bacteria, including *Lactobacillus* and *Akkermansia*, according to additional genus-level analysis, which was consistent with the effects of therapeutic *B. velezensis* HBXN2020.

Similarly, harmful bacteria such as *Alistipes*, *Bacteroides*, *Escherichia-Shigella*, and *Enterococcus* were significantly enriched in the PBS+STm group. A facultative-pathogenic bacterium called Alistipes encourages the

growth of inflammation, obesity, and colorectal cancer (Parker et al., 2020). Based on those results, we found that prophylactic *B. velezensis* HBXN2020 alleviates *S.* Typhimurium-induced colitis by increasing the abundance of beneficial bacteria, attenuating proinflammatory responses of the intestine, and increasing intestinal barrier function.

Conclusion

In conclusion, gut mucosal barrier disruption and intestinal inflammation results from dysbiosis of the colonic microbiota caused by S. Typhimurium ATCC14028 infection. Supplementing *Bacillus velezensis* HBXN2020 can improve intestinal microbiota stability and gut barrier integrity and reduce inflammation to help prevent or treat bacterial colitis.

Experimental procedures

Animals and bacterial strains.

Female specific-pathogen-free (SPF) C57BL/6 mice aged 6 to 8 weeks were purchased from the Animal Experimental Center of Huazhong Agricultural University. All mice experiments were conducted in the standard SPF facility of Huazhong Agricultural University, with 12 h of light and 12 h of darkness at a temperature of 25°C and ad libitum access to food and water. The use of animals in this experiment was approved by the Animal Care and

Ethics Committee of Huazhong Agricultural University (Ethics Approval Number: HZAUMO-2023-0089).

The strains used in this study are listed in Table S3, and all the primers used in Table S4. *Clostridium perfringens* were cultured in a fluid thioglycollate medium (FTG) (Hopebio, Qingdao, China) at 45°C. *Streptococcus suis* and *Pasteurella multocida* were cultured in tryptic soy broth (TSB) (BD Biosciences, MD, United States) medium supplemented with 5% (v/v) sheep serum (Solarbio, Beijing, China) at 37°C, and *Actinobacillus pleuropneumoniae* were cultured in TSB supplemented with 5% (v/v) sheep serum and 5mM nicotinamide adenine dinucleotide (NAD) at 37°C, while the other bacterial strains were cultured in Luria Bertani (LB) medium (Solarbio, Beijing, China) at 37°C. In addition, the Difco sporulation medium (DSM) was used for inducing the sporulation of *B. velezensis* HBXN2020 via the nutrient depletion method (Tang et al., 2017).

Stain isolation, growth conditions and strain identification.

In this study, we isolated 362 *Bacillus* strains from the feces of healthy piglets, and four *Bacillus* strains were screened through initial antibacterial tests. Then, a strain with broad-spectrum antimicrobial activity was ultimately screened out by the antibacterial spectrum assay (Table S5), and named as HBXN2020. The strain was stored in 28% glycerol at −80°C. For culturing the bacterial cells, Luria-Bertani (LB) media or agar plates supplemented with 1.5%

agar were used and incubated at 37°C.

A single bacterial colony was inoculated into 10 mL of LB medium and incubated overnight at 37°C with shaking (180 rpm). The bacteria genomic DNA was extracted using the TIANamp Genomic DNA Kit (TIANGEN, Beijing, China) from bacteria. Then, 16S ribosomal sequence was amplified using 16S-specific primers and sequenced to identify the HBXN2020.

Genome sequencing, annotation and analysis

The complete genome of *B. velezensis* HBXN2020 was sequenced using the Illumina HiSeq PE and PacBio RSII (SMRT) platforms (Shanghai Majorbio Bio-pharm Technology Co., Ltd.). Briefly, the short reads from the Illumina HiSeq PE were assembled into contigs using SPAdenovo (http://soap.genomics.org.cn/). The long reads from the PacBio RSII and the Illumina contigs were then aligned using the miniasm and Racon tools in Unicycler (version 0.4.8, https://github.com/rrwick/Unicycler) to generate long-read sequences. During the assembly process, sequence correction was performed using Pilon (version 1.22, https://github.com/broadinstitute/pilon/wiki/Standard-Output). Lastly, a complete genome with seamless chromosomes was obtained.

The coding sequences (CDs) of the *B. velezensis* HBXN2020 genome were predicted using Glimmer (version 3.02, http://ccb.jhu.edu/software/glimmer/index.shtml). The tRNA and rRNA genes

were predicted using TRNAscan-SE (version 2.0, http://trna.ucsc.edu/software/) and Barrnap (version 0.8, https://github.com/tseemann/barrnap), respectively. The functional annotation of all CDSs was performed using various databases, including Swiss-Prot Database (https://web.expasy.org/docs/swiss-prot_guideline.html), Pfam Database (http://pfam.xfam.org/), EggNOG Database (http://eggnog.embl.de/), GO Database (http://www.geneontology.org/), and KEGG Database (http://www.genome.jp/kegg/). The circular map of the *B. velezensis* HBXN2020 genome was generated using CGView (version 2, http://wishart.biology.ualberta.ca/cgview/) (Stothard and Wishart, 2005).

Comparative genomic analysis

To elucidate the phylogenetic relationships from a whole-genome perspective, a phylogenetic tree based on the whole genome was constructed using the Type (Strain) Genome Server (TYGS) online (https://ggdc.dsmz.de/) (Meier-Kolthoff et al., 2022). The average nucleotide identity (ANI) values of genome to genome were calculated using the JSpeciesWS online service (Richter et al., 2016), and a heatmap was then generated using TBtools (version 1.113) (Chen et al., 2020).

Growth curves of *B. velezensis* HBXN2020

The growth curve of *B. velezensis* HBXN2020 was recorded in flat-bottomed 100-well microtiter plates via detecting optical density at 600 nm

(OD_{600}) at 1 h intervals using the automatic growth curve analyzer (Bioscreen, Helsinki, Finland).

Antimicrobial Assays

The *in vitro* antagonistic activity of *B. velezensis* HBXN2020-CFS was tested using the agar well-diffusion method against 18 indicator strains (pathogens), which included 7 standard strains (*E. coli* ATCC 25922, *E. coli* ATCC 35150, *S.* Typhimurium ATCC 14028 (STm), *S.* Typhimurium SL1344, *S. aureus* ATCC 29213, *S. aureus* ATCC 43300, and *C. perfringens* CVCC 2030) and 11 clinical isolates (*E. coli* EC024, *S.* Enteritidis SE006, *S. aureus* S21, *C. perfringens* CP023, *C. perfringens* CP002, *S. suis* SC19, *S. suis* SS006, *P. multocida* PM002, *P. multocida* PM008, *A.* pleuropneumoniae APP015, and *A.* pleuropneumoniae APP017). All plates were cultured at 37°C for 16 h before observing the inhibition zone, and the diameter of the inhibition zone was measured using a vernier caliper. The presence of a clear zone indicated antagonistic activity.

Antibiotic susceptibility assays

Antimicrobial susceptibility testing was performed using the Kirby-Bauer (KB) disk diffusion method in accordance with the Clinical Laboratory Standards Institute (CLSI) guidelines (CLSI., 2018.). The antimicrobial agents tested were: Ampicillin, Meropenem, Piperacillin, Gentamycin, Tetracycline,

Doxycycline, Minocycline, Erythromycin, Enrofloxacin, Ofloxacin, Sulfamethoxazole, Trimethoprim-sulfamethoxazole, Polymyxin B, Teicoplanin, Trimethoprim, Florfenicol, Spectinomycin, Nitrofurantoin, and Rifampicin. The diameter of the inhibition zone was measured using a vernier caliper.

In vitro **resistance assay of** ***B. velezensis*** **HBXN2020**

B. velezensis HBXN2020 spores (100 μL) or vegetative cells (100 μL) were separately resuspended in 900 μL of LB medium supplemented with different pH values (2, 3, 4, 5 or 6), bile salts (0.85% NaCl, 0.3%), simulated gastric fluid (SGF, HCl, pH 1.2) containing 10 g L^{-1} of pepsin in 0.85% NaCl solution, or simulated intestinal fluid (SIF, NaOH, pH 6.8) containing 10 g L^{-1} of trypsin in 0.05 M KH2PO4 solution, and incubated at 37 °C. A normal LB medium (pH 7.0) was used as the control. At predetermined time points, 100 μL was taken from each sample, serially diluted 10-fold with sterile PBS (pH 7.2), and then spread onto LB agar plates. The plates were incubated overnight in a constant temperature incubator at 37°C, and the bacterial colonies were counted. The survival rate was calculated using the following formula: Survival rate = (number of bacteria in the treatment group/number of bacteria in the control group) × 100%.

One milliliter of *B. velezensis* HBXN2020 spores or vegetative cells were separately placed in water baths at different temperatures (37°C, 45°C, 55°C, 65°C, 75°C, 85°C or 95°C) for 20 min, with a 37°C water bath used as the

control. The survival rate was calculated as described above.

***In vitro* bacterial competition.**

To investigate whether *B. velezensis* HBXN2020 directly inhibited the growth of STm, we performed spot-on lawn and agar-well diffusion assays, as well as co-culture assays in liquid culture medium. In the spot-on lawn antimicrobial assays, we prepared double layers of agar by first pouring LB agar into the plate as the bottom layer. The top layer consisted of 10 mL TSB broth containing 0.7% agar with STm overnight culture. Then, 10 μL of *B. velezensis* HBXN2020 overnight culture and cell-free supernatant (CFS) were respectively spotted onto TSB agar and incubated at 37°C for 12 h to measure the inhibition zone. A transparent zone of at least 1 mm around the spot was considered positive.

The antagonistic effect of *B. velezensis* HBXN2020-CFS against STm was determined using the agar-well diffusion assays. To collect *B. velezensis* HBXN2020-CFS, the culture was centrifuged at 9,000g for 15 min at 4°C, and the supernatant was filtered through a 0.22 μm membrane filter (Millipore, USA). The STm lawn medium was prepared by mixing 10 mL of TSB broth containing 0.7% agar with STm overnight culture and then poured into a sterile plate covered with LB agar and Oxford cups, 8 mm diameter wells were prepared in the TSB agar after removing the cups. The wells were filled with 100 μL of *B. velezensis* HBXN2020-CFS, LB medium or ampicillin (100 μg

mL^{-1}). The plates were incubated at 37°C for 14 h, and the inhibition zone was measured.

The co-culture assay was conducted by incubating *B. velezensis* HBXN2020 and *S.* Typhimurium ATCC14028 (carry pET28a (+), kanamycin resistance) (Cao et al., 2019) separately overnight at 37°C and diluting them to 10^4 CFU/mL. Then, the two strains were mixed at different ratios (1:1, 1:10, 1:50 or 1:100) and co-cultured at 37°C with shaking (180 rpm). At predetermined time points, serial 10-fold dilutions were prepared for all samples and spread onto selective (kanamycin 50 μg mL^{-1}) LB agar plates and cultured at 37°C for 12 h before bacterial counting. Viable colony counts ranged from 30 to 300 per plate.

Biosafety assessment

Biosafety assay of *B. velezensis* HBXN2020 referred to the method described by Zhou et al.(Zhou et al., 2022) with slight modifications. After a 7-day acclimation period (free access to water and food), mice were randomly divided into four treatment groups (n = 5): low-dose *B. velezensis* HBXN2020 spores group (L-HBXN2020 group, 10^7 CFU/mouse), medium-dose *B. velezensis* HBXN2020 spores group (M-HBXN2020 group, 10^8 CFU/mouse), high-dose *B. velezensis* HBXN2020 spores group (H-HBXN2020 group, 10^9 CFU/mouse), and a control group. During the experimental period (15 days), mice were weighed and orally gavaged with their respective treatments once

every two days. On day 15, all mice were euthanized, and blood, heart, liver, spleen, lung, kidney, ileum, cecum, and colon were collected. Blood samples were used for routine blood and biochemistry tests. Major organ tissues (heart, liver, spleen, lung, and kidney) and a 5-mm distal segment of the colon were used for histopathology. The remaining colonic tissues were rapidly frozen in liquid nitrogen and stored at −80°C for cytokine and tight junction protein expression analysis.

***Salmonella* Typhimurium-induced mouse model of colitis.**

After 7 days of acclimation (free access to water and food), mice were randomly divided into three treatment groups (n = 8): Control group, STm + PBS group, and STm + HBXN2020 group. The *S.* Typhimurium-induced colitis was performed as previously described (Stecher et al., 2005), with slight modifications. On the first day of the experiment, all mice in the STm + PBS group and STm + HBXN2020 group were orally inoculated with 200 μL (5×10^7 CFU/mouse) of STm. On days 1, 3 and 5 following STm infection, each mouse in the STm + HBXN2020 group received 200 μL (1×10^8 CFU/mouse) of *B. velezensis* HBXN2020 spores via gavage administration. In contrast, the control group and STm + PBS group received 200 μL of sterile PBS by oral gavage. Fecal samples were collected daily following STm infection and resuspended in sterile PBS. The number of STm in mice feces from both the STm + PBS and STm + HBXN2020 groups was then determined by

682 spreading a serial 10-fold dilution on selective LB agar plates containing 50 μg
683 mL^{-1} kanamycin. Throughout the entire experiment, the body weight, stool
684 consistency and fecal occult blood of all mice were monitored daily. As shown
685 in Table S6, disease activity index (DAI) was calculated by the sum of the
686 scores from three parameters (Praveschotinunt et al., 2019). On day 7 after
687 STm infection, all mice were euthanized, their ileum, cecum and colon were
688 collected. The length of colon was measured, and a 5-mm distal segment of
689 the colon was fixed in 4% paraformaldehyde for further histopathology. The
690 remaining colon was then rapidly frozen in liquid nitrogen and stored at −80°C
691 for cytokine and tight junction protein expression analysis. Then, the number
692 of STm in the ileum, cecum, and colon was determined by spreading serial
693 10-fold dilutions on selective LB agar plates.

694 To investigate the prophylactic efficacy of *B. velezensis* HBXN2020 in
695 ameliorating STm-induced colitis, another independent experiment was
696 conducted using six-week-old female C57BL/6 mice (SPF). After a seven-day
697 acclimation period, mice were randomly assigned to three groups (n = 8):
698 control group, PBS + STm group and HBXN2020 + STm group. On days 1, 3,
699 5 and 7, each mouse in the HBXN2020 + STm group received 200 μL (1×10^8
700 CFU/mouse) of *B. velezensis* HBXN2020 spores via gavage administration.
701 Meanwhile, mice in the control group and PBS + STm group received 200 μL
702 of sterile PBS by oral gavage. On day 7, all mice in the PBS + STm group and
703 HBXN2020 + STm group were orally inoculated with 200 μL (5×10^7

CFU/mouse) of STm. Fecal samples were collected daily following STm infection from both groups and resuspended in sterile PBS. The number of STm in the feces of mice was then determined by spreading serial 10-fold dilutions on selective LB agar plates (50 μg mL^{-1} kanamycin). Throughout the entire experiment, the body weight and DAI scores of all mice were monitored daily. On day 12, all mice were euthanized, and the ileum, cecum, and colon were collected. The colon length was measured, and a 5-mm distal segment of the colon was fixed in 4% formalin for sectioning and staining. The remaining colon was stored at −80°C for future analysis. Lastly, the number of STm in the ileum, cecum, and colon was determined using a selective LB agar plate.

Determination of cytokines and tight junction protein expression in colon tissue

Total RNA was extracted from colon tissues using TRIpure reagent (Aidlab, China), and cDNA was obtained using HiScript® III RT SuperMix for qPCR (+gDNA wiper) (Vazyme, China). RT-qPCR for each gene was performed in triplicate using qPCR SYBR Green Master Mix (Yeasen Biotechnology, Shanghai, China). The relative expression level of cytokine and tight junction protein genes was calculated using the $2^{-\Delta\Delta Ct}$ method with β-actin and GAPDH as reference genes. The primer sequences used in the RT-qPCR test are listed in Table S4.

Histopathology analysis

Colon tissue samples (0.5 cm) were fixed in 4% paraformaldehyde for 24 h, and the fixed tissues were then embedded in paraffin and sectioned. The sections were stained with hematoxylin and eosin (H&E) and observed and imaged using an optical microscope (Olympus Optical, Tokyo, Japan). The histopathological score included the degree of inflammatory infiltration, changes in crypt structures, and the presence or absence of ulceration and edema. The scoring criteria were determined as previously described (Wu et al., 2022).

16S rRNA gene sequencing and analysis

According to the manufacturer's instructions, colon microbial community genomes were extracted using E.Z-N.A ® Stool DNA Kit (Omega; D4015-01), and quality was detected by 1% agarose gel electrophoresis. The 16S rRNA V3-V4 variable region was amplified by PCR using universal primers 338F (5 '- ACTCCTACGGGGGGCAG-3') and 806R (5 '- GACTACHVGGGTWTCTAAT-3'). The PCR products were examined by electrophoresis on 2% agarose gels and then purified with the AxyPrep DNA gel extraction kit (Axygen Biosciences, USA). A sequencing library was constructed using the NEXTFLEX® Rapid DNA-Seq Kit, and sequencing was performed using the Illumina MiSeq platform. Raw reads were quality

evaluated and filtered by fastp (version 0.20.0) and merged using FLASH (version 1.2.7). The optimized sequences were clustered into operational taxonomic units (OTUs) based on 97% sequence similarity using UPARSE (version 7.1). The representative sequences of each OTU was classified by RDP classifier (version 2.2; confidence threshold value, 0.7). Alpha diversity was assessed using the ACE, chao, Shannon, and Simpson indices. The β-diversity analysis was performed using Bray-Curtis distances and visualized through principal component analysis (PCA). Linear discriminant analysis (LDA) effect size (LefSe) was used to identify differential microbiota between groups.

Statistical Analysis

Statistical analysis was performed using GraphPad Prism 8.3.0 (GraphPad Software, San Diego, CA, USA) and Excel (Microsoft, Redmond, USA). Data are presented as mean ± standard error of the mean (SEM). Differences between two groups were evaluated using two-tailed unpaired Student's t-test, and all other comparisons were conducted using one-way analysis of variance (ANOVA) with Tukey's multiple comparisons test. For all analyses, significance differences are denoted as: *, $P < 0.05$, **, $P < 0.01$, and ***, $P < 0.001$.

Data availability

The datasets supporting the conclusions of this article were deposited in the NCBI Sequence Read Archive database under the accession numbers: CP119399.1 (whole genome sequencing raw data) and PRJNA1045315 (microbiota raw sequencing data).

Conflict of interest: We declare no conflict of interest.

ACKNOWLEDGMENTS

This work was supported by grants from the National Program on Key Research Project of China (2021YFD1800300, 2022YFD1800800), “Yingzi Tech & Huazhong Agricultural University Intelligent Research Institute of Food Health” (No. IRIFH202209; IRIFH202301), and the Fundamental Research Funds for the Central Universities (2662016PY004).

Author contributions

Linkang Wang: Conceptualization, Methodology, Data curation, Formal analysis, Writing - original draft. **Haiyan Wang, Xinxin Li, Mengyuan Zhu**: Methodology, Data curation, Planned and performed the experiments. **Dongyang Gao, Dayue Hu, Zhixuan Xiong**: Methodology, Writing - Reviewing and Editing. **Xiangmin Li**: Supervision, Writing-reviewing and editing. **Ping Qian**: Conceptualization, Funding acquisition, Project administration, Supervision, Writing-Reviewing and Editing. All authors read

and approved the submitted version of the paper.

Funding information

This work was supported by grants from the National Program on Key Research Project of China (2021YFD1800300, 2022YFD1800800), "Yingzi Tech & Huazhong Agricultural University Intelligent Research Institute of Food Health" (No. IRIFH202209; IRIFH202301), and the Fundamental Research Funds for the Central Universities (2662016PY004).

Reference

Abdhul, K., Ganesh, M., Shanmughapriya, S., Vanithamani, S., Kanagavel, M., Anbarasu, K., and Natarajaseenivasan, K. (2015). Bacteriocinogenic potential of a probiotic strain Bacillus coagulans [BDU3] from Ngari. Int J Biol Macromol *79*, 800-806.

Bazzoni, G., Martinez-Estrada, O.M., Orsenigo, F., Cordenonsi, M., Citi, S., and Dejana, E. (2000). Interaction of junctional adhesion molecule with the tight junction components ZO-1, cingulin, and occludin. J Biol Chem *275*, 20520-20526.

Cani, P.D., Depommier, C., Derrien, M., Everard, A., and de Vos, W.M. (2022). Akkermansia muciniphila: paradigm for next-generation beneficial microorganisms. Nat Rev Gastroenterol Hepatol *19*, 625-637.

Cao, Z., Wang, X., Pang, Y., Cheng, S., and Liu, J. (2019). Biointerfacial self-assembly generates lipid membrane coated bacteria for enhanced oral delivery and treatment. Nat Commun *10*, 5783.

Chen, C., Chen, H., Zhang, Y., Thomas, H.R., Frank, M.H., He, Y., and Xia, R. (2020). TBtools: An Integrative Toolkit Developed for Interactive Analyses of Big Biological Data. Mol Plant *13*, 1194-1202.

Chen, L., Wang, D., Garmaeva, S., Kurilshikov, A., Vich Vila, A., Gacesa, R., Sinha, T., Segal, E., Weersma, R.K., Wijmenga, C., *et al.* (2021). The long-term genetic stability and individual specificity of the human gut microbiome. Cell *184*, 2302-2315.e2312.

Cheng, A., Yan, H., Han, C., Wang, W., Tian, Y., and Chen, X. (2014). Polyphenols from blueberries modulate inflammation cytokines in LPS-induced RAW264.7 macrophages. Int J Biol Macromol *69*, 382-387.

CLSI. (2018.). Performance standards for antimicrobial disk susceptibility tests, M02, 13th ed. Clinical and Laboratory Standards Institute, Wayne, PA.

Cristofori, F., Dargenio, V.N., Dargenio, C., Miniello, V.L., Barone, M., and Francavilla, R. (2021). Anti-Inflammatory and Immunomodulatory Effects of Probiotics in Gut Inflammation: A Door to the Body. Front Immunol *12*, 578386.

Crits-Christoph, A., Hallowell, H.A., Koutouvalis, K., and Suez, J. (2022). Good microbes, bad genes?

826 The dissemination of antimicrobial resistance in the human microbiome. Gut Microbes *14*, 2055944.
827 Cross, A.S., Sadoff, J.C., Kelly, N., Bernton, E., and Gemski, P. (1989). Pretreatment with recombinant
828 murine tumor necrosis factor alpha/cachectin and murine interleukin 1 alpha protects mice from
829 lethal bacterial infection. J Exp Med *169*, 2021-2027.
830 Dinarello, C.A. (2000). Proinflammatory cytokines. Chest *118*, 503-508.
831 Du, H., Yao, W., Kulyar, M.F., Ding, Y., Zhu, H., Pan, H., Li, K., Bhutta, Z.A., Liu, S., and Li, J. (2022). Effects
832 of Bacillus amyloliquefaciens TL106 Isolated from Tibetan Pigs on Probiotic Potential and Intestinal
833 Microbes in Weaned Piglets. Microbiol Spectr *10*, e0120521.
834 Fabrega, A., and Vila, J. (2013). Salmonella enterica serovar Typhimurium skills to succeed in the host:
835 virulence and regulation. Clin Microbiol Rev *26*, 308-341.
836 Ferri, M., Ranucci, E., Romagnoli, P., and Giaccone, V. (2017). Antimicrobial resistance: A global
837 emerging threat to public health systems. Crit Rev Food Sci Nutr *57*, 2857-2876.
838 Gou, S., Chen, N., Wu, X., Zu, M., Yi, S., Ying, B., Dai, F., Ke, B., and Xiao, B. (2022). Multi-responsive
839 nanotheranostics with enhanced tumor penetration and oxygen self-producing capacities for
840 multimodal synergistic cancer therapy. Acta Pharm Sin B *12*, 406-423.
841 Gu, S.B., Zhao, L.N., Wu, Y., Li, S.C., Sun, J.R., Huang, J.F., and Li, D.D. (2015). Potential probiotic
842 attributes of a new strain of Bacillus coagulans CGMCC 9951 isolated from healthy piglet feces. World
843 J Microbiol Biotechnol *31*, 851-863.
844 Hardt, W.D., Chen, L.M., Schuebel, K.E., Bustelo, X.R., and Galán, J.E. (1998). S. typhimurium encodes
845 an activator of Rho GTPases that induces membrane ruffling and nuclear responses in host cells. Cell
846 *93*, 815-826.
847 Hayashi, A., Sato, T., Kamada, N., Mikami, Y., Matsuoka, K., Hisamatsu, T., Hibi, T., Roers, A., Yagita, H.,
848 Ohteki, T., *et al.* (2013). A single strain of Clostridium butyricum induces intestinal IL-10-producing
849 macrophages to suppress acute experimental colitis in mice. Cell Host Microbe *13*, 711-722.
850 Herp, S., Brugiroux, S., Garzetti, D., Ring, D., Jochum, L.M., Beutler, M., Eberl, C., Hussain, S., Walter, S.,
851 Gerlach, R.G., *et al.* (2019). Mucispirillum schaedleri Antagonizes Salmonella Virulence to Protect Mice
852 against Colitis. Cell Host Microbe *25*, 681-694 e688.
853 Huang, F.C. (2009). Upregulation of Salmonella-induced IL-6 production in Caco-2 cells by PJ-34, PARP-
854 1 inhibitor: involvement of PI3K, p38 MAPK, ERK, JNK, and NF-kappaB. Mediators Inflamm *2009*,
855 103890.
856 Karki, R., Sharma, B.R., Tuladhar, S., Williams, E.P., Zalduondo, L., Samir, P., Zheng, M., Sundaram, B.,
857 Banoth, B., Malireddi, R.K.S., *et al.* (2021). Synergism of TNF-alpha and IFN-gamma Triggers
858 Inflammatory Cell Death, Tissue Damage, and Mortality in SARS-CoV-2 Infection and Cytokine Shock
859 Syndromes. Cell *184*, 149-168 e117.
860 Katiyo, S., Muller-Pebody, B., Minaji, M., Powell, D., Johnson, A.P., De Pinna, E., Day, M., Harris, R., and
861 Godbole, G. (2019). Epidemiology and Outcomes of Nontyphoidal Salmonella Bacteremias from
862 England, 2004 to 2015. J Clin Microbiol *57*.
863 Kaur, H., Gupta, T., Kapila, S., and Kapila, R. (2021). Protective effects of potential probiotic
864 Lactobacillus rhamnosus (MTCC-5897) fermented whey on reinforcement of intestinal epithelial
865 barrier function in a colitis-induced murine model. Food Funct *12*, 6102-6116.
866 Kotas, M.E., and Medzhitov, R. (2015). Homeostasis, inflammation, and disease susceptibility. Cell *160*,
867 816-827.
868 Li, A., Wang, Y., Li, Z., Qamar, H., Mehmood, K., Zhang, L., Liu, J., Zhang, H., and Li, J. (2019). Probiotics
869 isolated from yaks improves the growth performance, antioxidant activity, and cytokines related to

870 immunity and inflammation in mice. Microb Cell Fact *18*, 112.
871 Liu, C., Chu, D., Kalantar-Zadeh, K., George, J., Young, H.A., and Liu, G. (2021). Cytokines: From Clinical
872 Significance to Quantification. Adv Sci (Weinh) *8*, e2004433.
873 Maloy, K.J., and Powrie, F. (2011). Intestinal homeostasis and its breakdown in inflammatory bowel
874 disease. Nature *474*, 298-306.
875 Meier-Kolthoff, J.P., Carbasse, J.S., Peinado-Olarte, R.L., and Goker, M. (2022). TYGS and LPSN: a
876 database tandem for fast and reliable genome-based classification and nomenclature of prokaryotes.
877 Nucleic Acids Res *50*, D801-D807.
878 Mohan, A., Munusamy, C., Tan, Y.C., Muthuvelu, S., Hashim, R., Chien, S.L., Wong, M.K., Khairuddin,
879 N.A., Podin, Y., Lau, P.S., *et al.* (2019). Invasive Salmonella infections among children in Bintulu,
880 Sarawak, Malaysian Borneo: a 6-year retrospective review. BMC Infect Dis *19*, 330.
881 Morgan, K.L. (2013). Infection, illness, and fenugreek seeds: was illness a good enough proxy for
882 infection in the 2011 outbreak of shiga toxin-producing Escherichia coli O104:H4 in France? Clin Infect
883 Dis *56*, 1055-1056.
884 Ohland, C.L., and Macnaughton, W.K. (2010). Probiotic bacteria and intestinal epithelial barrier
885 function. Am J Physiol Gastrointest Liver Physiol *298*, G807-819.
886 Ouattara, H.G., Reverchon, S., Niamke, S.L., and Nasser, W. (2017). Regulation of the synthesis of pulp
887 degrading enzymes in Bacillus isolated from cocoa fermentation. Food Microbiol *63*, 255-262.
888 Ouyang, W., Rutz, S., Crellin, N.K., Valdez, P.A., and Hymowitz, S.G. (2011). Regulation and functions of
889 the IL-10 family of cytokines in inflammation and disease. Annu Rev Immunol *29*, 71-109.
890 Ozer, J., Ratner, M., Shaw, M., Bailey, W., and Schomaker, S. (2008). The current state of serum
891 biomarkers of hepatotoxicity. Toxicology *245*, 194-205.
892 Parker, B.J., Wearsch, P.A., Veloo, A.C.M., and Rodriguez-Palacios, A. (2020). The Genus Alistipes: Gut
893 Bacteria With Emerging Implications to Inflammation, Cancer, and Mental Health. Front Immunol *11*,
894 906.
895 Paulson, J.A., Zaoutis, T.E., Council on Environmental, H., and Committee on Infectious, D. (2015).
896 Nontherapeutic Use of Antimicrobial Agents in Animal Agriculture: Implications for Pediatrics.
897 Pediatrics *136*, e1670-1677.
898 Pickard, J.M., Zeng, M.Y., Caruso, R., and Núñez, G. (2017). Gut microbiota: Role in pathogen
899 colonization, immune responses, and inflammatory disease. Immunol Rev *279*, 70-89.
900 Polk, B.F., and Kasper, D.L. (1977). Bacteroides fragilis subspecies in clinical isolates. Ann Intern Med *86*,
901 569-571.
902 Praveschotinunt, P., Duraj-Thatte, A.M., Gelfat, I., Bahl, F., Chou, D.B., and Joshi, N.S. (2019).
903 Engineered E. coli Nissle 1917 for the delivery of matrix-tethered therapeutic domains to the gut. Nat
904 Commun *10*, 5580.
905 Reyman, M., van Houten, M.A., Watson, R.L., Chu, M., Arp, K., de Waal, W.J., Schiering, I., Plotz, F.B.,
906 Willems, R.J.L., van Schaik, W., *et al.* (2022). Effects of early-life antibiotics on the developing infant gut
907 microbiome and resistome: a randomized trial. Nat Commun *13*, 893.
908 Richter, M., Rossello-Mora, R., Oliver Glockner, F., and Peplies, J. (2016). JSpeciesWS: a web server for
909 prokaryotic species circumscription based on pairwise genome comparison. Bioinformatics *32*, 929-
910 931.
911 Sanders, M.E., Akkermans, L.M., Haller, D., Hammerman, C., Heimbach, J., Hormannsperger, G., Huys,
912 G., Levy, D.D., Lutgendorff, F., Mack, D., *et al.* (2010). Safety assessment of probiotics for human use.
913 Gut Microbes *1*, 164-185.

914 Saraiva, M., Vieira, P., and O'Garra, A. (2020). Biology and therapeutic potential of interleukin-10. J Exp
915 Med *217*.
916 Schultz, B.M., Paduro, C.A., Salazar, G.A., Salazar-Echegarai, F.J., Sebastian, V.P., Riedel, C.A., Kalergis,
917 A.M., Alvarez-Lobos, M., and Bueno, S.M. (2017). A Potential Role of Salmonella Infection in the Onset
918 of Inflammatory Bowel Diseases. Front Immunol *8*, 191.
919 Shao, J., Liu, Y., Xie, J., Stefanic, P., Lv, Y., Fan, B., Mandic-Mulec, I., Zhang, R., Shen, Q., and Xu, Z.
920 (2022). Annulment of Bacterial Antagonism Improves Plant Beneficial Activity of a Bacillus velezensis
921 Consortium. Appl Environ Microbiol *88*, e0024022.
922 Singhal, M., Liu, X., Inverso, D., Jiang, K., Dai, J., He, H., Bartels, S., Li, W., Abdul Pari, A.A.,
923 Gengenbacher, N., *et al.* (2018). Endothelial cell fitness dictates the source of regenerating liver
924 vasculature. J Exp Med *215*, 2497-2508.
925 Snydman, D.R. (2008). The safety of probiotics. Clin Infect Dis *46 Suppl 2*, S104-111; discussion S144-
926 151.
927 Stecher, B., Macpherson, A.J., Hapfelmeier, S., Kremer, M., Stallmach, T., and Hardt, W.D. (2005).
928 Comparison of Salmonella enterica serovar Typhimurium colitis in germfree mice and mice pretreated
929 with streptomycin. Infect Immun *73*, 3228-3241.
930 Stothard, P., and Wishart, D.S. (2005). Circular genome visualization and exploration using CGView.
931 Bioinformatics *21*, 537-539.
932 Tang, Y., Gao, C., Xing, M., Li, Y., Zhu, L., Wang, D., Yang, X., Liu, L., and Yao, P. (2012). Quercetin
933 prevents ethanol-induced dyslipidemia and mitochondrial oxidative damage. Food Chem Toxicol *50*,
934 1194-1200.
935 Tang, Z., Sun, H., Chen, T., Lin, Z., Jiang, H., Zhou, X., Shi, C., Pan, H., Chang, O., Ren, P., *et al.* (2017).
936 Oral delivery of Bacillus subtilis spores expressing cysteine protease of Clonorchis sinensis to grass
937 carp (Ctenopharyngodon idellus): Induces immune responses and has no damage on liver and
938 intestine function. Fish Shellfish Immunol *64*, 287-296.
939 Wang, L., Gou, X., Ding, Y., Liu, J., Wang, Y., Wang, Y., Zhang, J., Du, L., Peng, W., and Fan, G. (2023). The
940 interplay between herbal medicines and gut microbiota in metabolic diseases. Front Pharmacol *14*,
941 1105405.
942 Wang, Y., Xie, Q., Zhang, Y., Ma, W., Ning, K., Xiang, J.Y., Cui, J., and Xiang, H. (2020). Combination of
943 probiotics with different functions alleviate DSS-induced colitis by regulating intestinal microbiota, IL-
944 10, and barrier function. Appl Microbiol Biotechnol *104*, 335-349.
945 Wu, J., Lin, Z., Wang, X., Zhao, Y., Zhao, J., Liu, H., Johnston, L.J., Lu, L., and Ma, X. (2022).
946 Limosilactobacillus reuteri SLZX19-12 Protects the Colon from Infection by Enhancing Stability of the
947 Gut Microbiota and Barrier Integrity and Reducing Inflammation. Microbiol Spectr *10*, e0212421.
948 Yang, W., Liu, Z., Zhao, Q., Du, H., Yu, J., Wang, H., Liu, X., Liu, H., Jing, X., Yang, H., *et al.* (2022).
949 Population Genetic Structure and Selection Signature Analysis of Beijing Black Pig. Front Genet *13*,
950 860669.
951 Yang, W.H., Westman, J.S., Heithoff, D.M., Sperandio, M., Cho, J.W., Mahan, M.J., and Marth, J.D.
952 (2021). Neu3 neuraminidase induction triggers intestinal inflammation and colitis in a model of
953 recurrent human food-poisoning. Proc Natl Acad Sci U S A *118*.
954 Ye, M., Tang, X., Yang, R., Zhang, H., Li, F., Tao, F., Li, F., and Wang, Z. (2018). Characteristics and
955 Application of a Novel Species of Bacillus: Bacillus velezensis. ACS Chem Biol *13*, 500-505.
956 Zhang, D.X., Kang, Y.H., Zhan, S., Zhao, Z.L., Jin, S.N., Chen, C., Zhang, L., Shen, J.Y., Wang, C.F., Wang,
957 G.Q., *et al.* (2019). Effect of Bacillus velezensis on Aeromonas veronii-Induced Intestinal Mucosal

Barrier Function Damage and Inflammation in Crucian Carp (Carassius auratus). Front Microbiol *10*, 2663.

Zhang, L., Bai, K., Zhang, J., Xu, W., Huang, Q., and Wang, T. (2017). Dietary effects of Bacillus subtilis fmbj on the antioxidant capacity of broilers at an early age. Poult Sci *96*, 3564-3573.

Zhou, J., Li, M., Chen, Q., Li, X., Chen, L., Dong, Z., Zhu, W., Yang, Y., Liu, Z., and Chen, Q. (2022). Programmable probiotics modulate inflammation and gut microbiota for inflammatory bowel disease treatment after effective oral delivery. Nat Commun *13*, 3432.

Zihni, C., Mills, C., Matter, K., and Balda, M.S. (2016). Tight junctions: from simple barriers to multifunctional molecular gates. Nat Rev Mol Cell Biol *17*, 564-580.

Figure legends

Fig. 1 Genomic characteristics and phylogenetic relationships of *B. velezensis* HBXN2020. (**A**) The whole-genome map of *B. velezensis* HBXN2020 with its genomic features. The map consists of 6 circles. From the inner circle to the outer circle: (1) GC-skew, (2) GC content, (3) reverse protein-coding genes, different colors represents different COG functional classifications, (4) genes transcribed in reverse direction, (5) genes transcribed in forward direction, (6) forward protein-coding genes, different colors represents different COG functional classifications. (**B**) The whole genome phylogenetic tree was constructed based on genome-wide data from 14 bacillus strains. *B. velezensis* HBXN2020 are indicated in bold.

Fig. 2 Growth curve of *B. velezensis* HBXN2020 and its *in vitro* resistance against environmental assaults. (**A**) Growth curves of *B. velezensis* HBXN2020 cultured in LB medium at 37°C, detection of OD_{600}

values at 1 h intervals in microplate reader. (**B**) Survival rate of endospore and vegetative cells of *B. velezensis* HBXN2020 after 30 min at different temperatures (37°C, 45°C, 55°C, 65°C, 75°C, 85°C or 95°C). Equal amounts of endospore and vegetative cells of HBXN2020 were exposed to the following: (**C**) acid solution (pH 2 to 7), (**D**) 0.3% bile salts, (**E**) SGF (pH 1.2) supplemented with pepsin, and (**F**) SIF (pH 6.8) containing trypsin at 37°C. At predetermined time points, 100 μL was taken from each sample, and tenfold serially diluted with sterile PBS (pH 7.2), and then spread on LB agar plates and cultured at 37°C for 12 h before bacterial counting. Each group was repeated three times (n = 3).

Fig. 3 Antibiotic susceptibility of *B. velezensis* HBXN2020 and bacteriostasis assay *in vitro*. (**A**) The diameter of the antibacterial zone indicates the extent of sensitivity to antibiotics. (**B**) The diameter of the antibacterial zone indicates the extent of inhibition against pathogenic bacteria. The diameter of the antibacterial zone was measured with vernier caliper. Each group was repeated three times (n = 3). R, resistant; I, moderately sensitive; S, sensitive.

Fig. 4 *In vivo* safety evaluation of *B. velezensis* HBXN2020 in a mouse model. (**A**) Body weights changes of mice during gavage with *B. velezensis* HBXN2020 spores. Mice were treated with sterile PBS (Control group) or low-

dose (L-HBXN2020 group), medium dose (M-HBXN2020 group), and high-dose (H-HBXN2020 group) of *B. velezensis* HBXN2020 spores. Weighing and gavage were performed once every two days during the experimental period (15 days). Data were shown as mean values ± SEM (n = 5). (**B**) The relative gene expression levels of inflammatory cytokines in the colon of mice measured by RT-qPCR. Data were shown as mean values ± SEM (n = 5). (**C**) The relative gene expression levels of barrier protein ZO-1, occludin, claudin and Muc2 in the colon of mice measured by RT-qPCR. Data were shown as mean values ± SEM (n = 5). (**D**) Major blood routine parameters and (**E**) serum biochemical parameters of mice in the control group and H-HBXN2020 group. Data were shown as mean values ± SEM (n = 3). (**F**) H&E stained colon sections in the different groups. Scale bar: 200 μm.

Fig. 5 Oral *B. velezensis* HBXN2020 spores alleviated *S.* Typhimurium-induced experimental mouse colitis. (**A**) *In vitro* Bacterial competition between STm and *B. velezensis* HBXN2020. STm were co-incubated with *B. velezensis* HBXN2020 at various ratios at 37°C with shaking. The growth of STm was reflected by bacterial counting per hour. (**B**) Experimental design for treatment in this study. Orally administrated with either PBS, or *B. velezensis* HBXN2020 spores by gavage at days 1, 3, and 5 after STm infection (5×10^7 CFU/mouse), respectively. All mice were euthanized at day 7 after STm infection. (**C**) Bacterial count of STm in mouse feces. Fecal samples were

collected per day after STm infection and resuspended in sterile PBS (0.1 g of fecal resuspended in 1 mL of sterile PBS). One hundred microliters of each sample performed a serial of 10-fold dilutions and spread on selective agar plates (50 μg mL^{-1} kanamycin) and incubated at 37°C for 12 h before bacterial counting. The bacterial loads of STm in (**D**) ileum, (**E**) cecum, and (**F**) colon. The cecum and colon were harvested and then homogenized. Statistical signifcance was evaluated using Student's t-test (*, $P < 0.05$, **, $P < 0.01$, and ***, $P < 0.001$). (**G**) Daily body weight changes and (**H**) daily disease activity index (DAI) scores of mice with different treatment groups. Data were shown as mean values ± SEM (n = 8). Statistical signifcance was evaluated using one-way analysis of variance (ANOVA) with Tukey's multiple comparisons test. *, $P < 0.05$, **, $P < 0.01$, and ***, $P < 0.001$ relative to Control group; $^{\#}$, $P < 0.05$, $^{\#\#}$, $P < 0.01$, $^{\#\#\#}$, $P < 0.001$ relative to STm + HBXN2020 group. (**I**) Colonic tissue images. (**J**) The length of the colon from per group (n = 8). Statistical signifcance was evaluated using one-way analysis of variance (ANOVA) with Tukey's multiple comparisons test (*, $P < 0.05$, **, $P < 0.01$, and ***, $P < 0.001$).

Fig. 6 Oral *B. velezensis* HBXN2020 spores attenuated colonic damage and inflammatory reaction. (**A**) H&E stained colon tissue sections. Scale bar: 200 μm. The relative gene expression levels of TNF-α (**B**), IL-1β (**C**), IL-6 (**D**), and IL-10 (**E**) were detected by RT-qPCR. Data were shown as mean values

± SEM (n = 6). The relative gene expression levels of ZO-1 (**F**), ocludin (**G**), claudin (**H**), and Muc2 (**I**) in colon tissue were detected by RT-qPCR. Data were shown as mean values ± SEM (n = 6). Statistical signifcance was evaluated using one-way analysis of variance (ANOVA) with Tukey's multiple comparisons test (*, $P < 0.05$, **, $P < 0.01$, and ***, $P < 0.001$).

Fig. 7 Oral *B. velezensis* HBXN2020 spores regulated the composition of intestinal microbiota. The α-diversity of the gut microbiota, determined by the (**A**) Sobs, (**B**) Chao1, (**C**) Shannon, and (**D**) Simpson diversity index. Data were shown as mean values ± SEM (n = 5). (**E**) The PCA plot showed the β-diversity of the gut microbiota based on Bray-Curtis distance at the OTU level. Heatmap of the community composition of colonic microbiota at the phylum (top 10 phyla) (**F**) and genus (top 30 genera) (**G**) level. Relative abundance of selected taxa (**H**) *norank_f_Muribaculaceae*, (**I**) *Lactobacillus*, (**J**) *Bacteroides*, and (**K**) *Escherichia-Shigella*. (**L**) Analysis of differences in the microbial communities by LEfSe (linear discriminant analysis (LDA score > 3.5) among different groups. Signifcance was evaluated by the Kruskal-Wallis test or ANOVA with Tukey's multiple comparisons test (*, P < 0.05, **, P < 0.01, and ***, P < 0.001).

Fig. 8 Prophylactic *B. velezensis* HBXN2020 spores attenuated the symptoms of *S.* Typhimurium-induced mouse colitis. (**A**) Experimental

design for treatment in this study. At days 1, 3, 5, and 7, each mouse in the HBXN2020 + STm group and PBS + STm group were received 200 μL (1×10^8 CFU/mouse) of *B. velezensis* HBXN2020 spores or sterile PBS by gavage. Then, mice in PBS + STm group and HBXN2020 + STm group were orally inoculated with 200 μL (5×10^7 CFU/mouse) of STm on day 7. On day 12, all mice were euthanized. (**B**) Daily body weight changes and (**C**) daily disease activity index (DAI) scores of mice with different groups following STm treatment. Data were shown as mean values ± SEM (n = 8). Statistical signifcance was evaluated using one-way analysis of variance (ANOVA) with Tukey's multiple comparisons test. *, $P < 0.05$, **, $P < 0.01$, and ***, $P < 0.001$ relative to Control group; $^{\#}$, $P < 0.05$, $^{\#\#}$, $P < 0.01$, $^{\#\#\#}$, $P < 0.001$ relative to HBXN2020 + STm group. (**D**) Colonic tissue images. (**E**) The length of the colon from per group (n = 8). (**F**) Bacterial count of STm in mouse feces. Fecal samples were collected every day after STm infection and resuspended in sterile PBS (0.1 g of fecal resuspended in 1 mL of sterile PBS). One hundred microliters of each sample performed a serial of 10-fold dilutions and spread on selective agar plates (50 μg mL^{-1} kanamycin) and incubated at 37°C for 12 h before bacterial counting. The bacterial loads of STm in (**G**) cecum and (**H**) colon. The cecum and colon were harvested and then homogenized. Statistical signifcance was evaluated using Student's t-test (*, $P < 0.05$, **, $P < 0.01$, and ***, $P < 0.001$).

Fig. 9 Prophylactic *B. velezensis* HBXN2020 spores attenuated colonic damage and inflammatory reaction. (**A**) H&E stained colon tissue sections. Scale bar: 200 μm. The relative gene expression levels of TNF-α (**B**), IL-1β (**C**), IL-6 (**D**), and IL-10 (**E**) were detected by RT-qPCR. Data were shown as mean values ± SEM (n = 6). The relative gene expression levels of ZO-1 (**F**), ocludin (**G**), claudin (**H**), and Muc2 (**I**) in colon tissue were detected by RT-qPCR. Data were shown as mean values ± SEM (n = 6). Statistical signifcance was evaluated using one-way analysis of variance (ANOVA) with Tukey's multiple comparisons test (*, $P < 0.05$, **, $P < 0.01$, and ***, $P < 0.001$).

Fig. 10 Prophylactic *B. velezensis* HBXN2020 spores regulated the composition of gut microbiota. (**A** to **D**) Alpha diversity of the intestinal microbiota. Data were shown as mean values ± SEM (n = 5). (**E**) The PCA plot showed the β-diversity among different microbial community groups based on Bray-Curtis distance at the OTU level. Heatmap of the community composition of colonic microbiota at the phylum (top 10 phyla) (**F**) and genus (top 30 genera) (**G**) level. Relative abundance of selected taxa (**H**) *Lactobacillus*, (**I**) *Akkermansia*, (**J**) *Alistipes*, (**K**) *Bacteroides*, (**L**) *Escherichia-Shigella*, and (**M**) *Enterococcus*. Data were shown as mean values ± SEM (n = 5). (**N**) Analysis of differences in the microbial taxa by LEfSe (LDA score > 3.5) in different groups. Signifcance was evaluated by the Kruskal-Wallis test or ANOVA with Tukey's multiple comparisons test (*, P < 0.05, **, P < 0.01,

1116 and ***, $P < 0.001$).

A

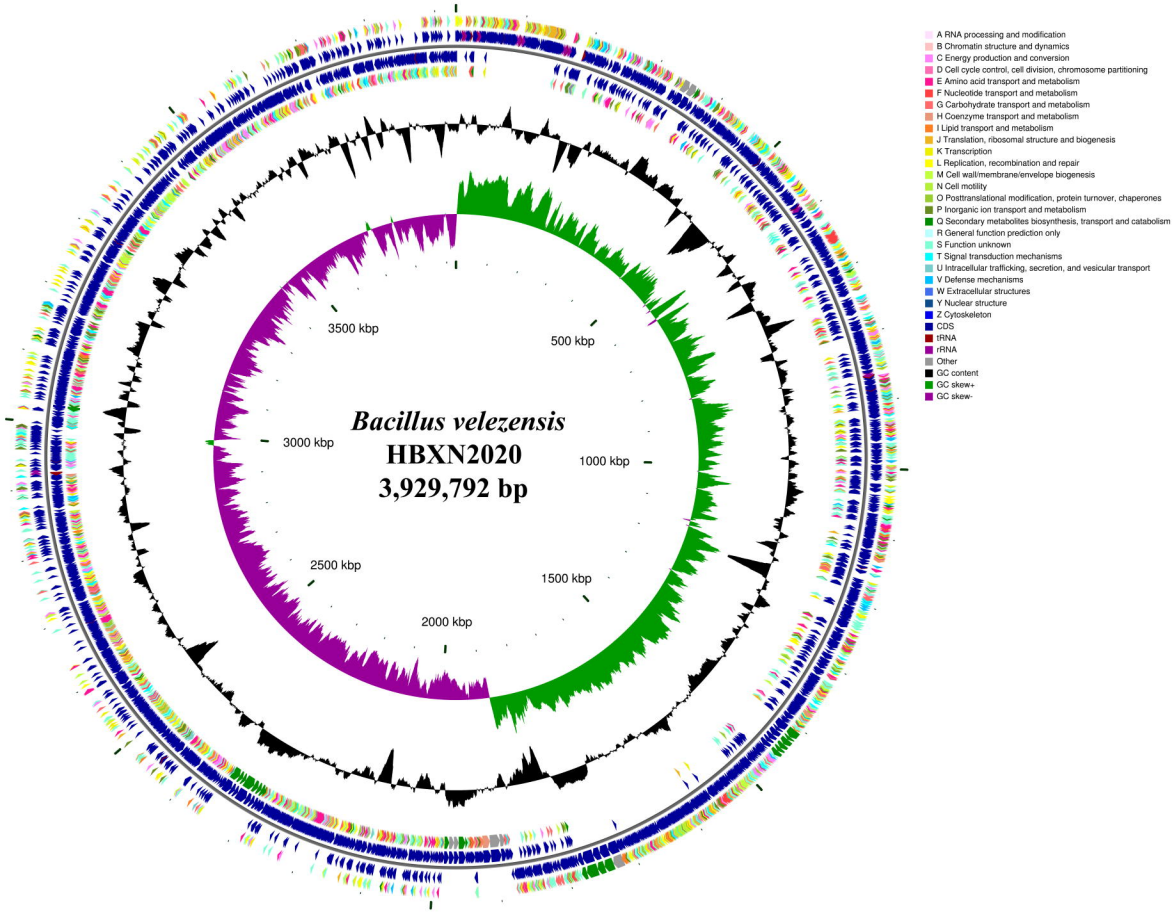
A RNA processing and modification
B Chromatin structure and dynamics
C Energy production and conversion
D Cell cycle control, cell division, chromosome partitioning
E Amino acid transport and metabolism
F Nucleotide transport and metabolism
G Carbohydrate transport and metabolism
H Coenzyme transport and metabolism
I Lipid transport and metabolism
J Translation, ribosomal structure and biogenesis
K Transcription
L Replication, recombination and repair
M Cell wall/membrane/envelope biogenesis
N Cell motility
O Posttranslational modification, protein turnover, chaperones
P Inorganic ion transport and metabolism
Q Secondary metabolites biosynthesis, transport and catabolism
R General function prediction only
S Function unknown
T Signal transduction mechanisms
U Intracellular trafficking, secretion, and vesicular transport
V Defense mechanisms
W Extracellular structures
Y Nuclear structure
Z Cytoskeleton
CDS
tRNA
rRNA
Other
GC content
GC skew+
GC skew-
3500 kbp
500 kbp
Bacillus velezensis
HBXN2020
3,929,792 bp
3000 kbp
1000 kbp
2500 kbp
1500 kbp
2000 kbp

B

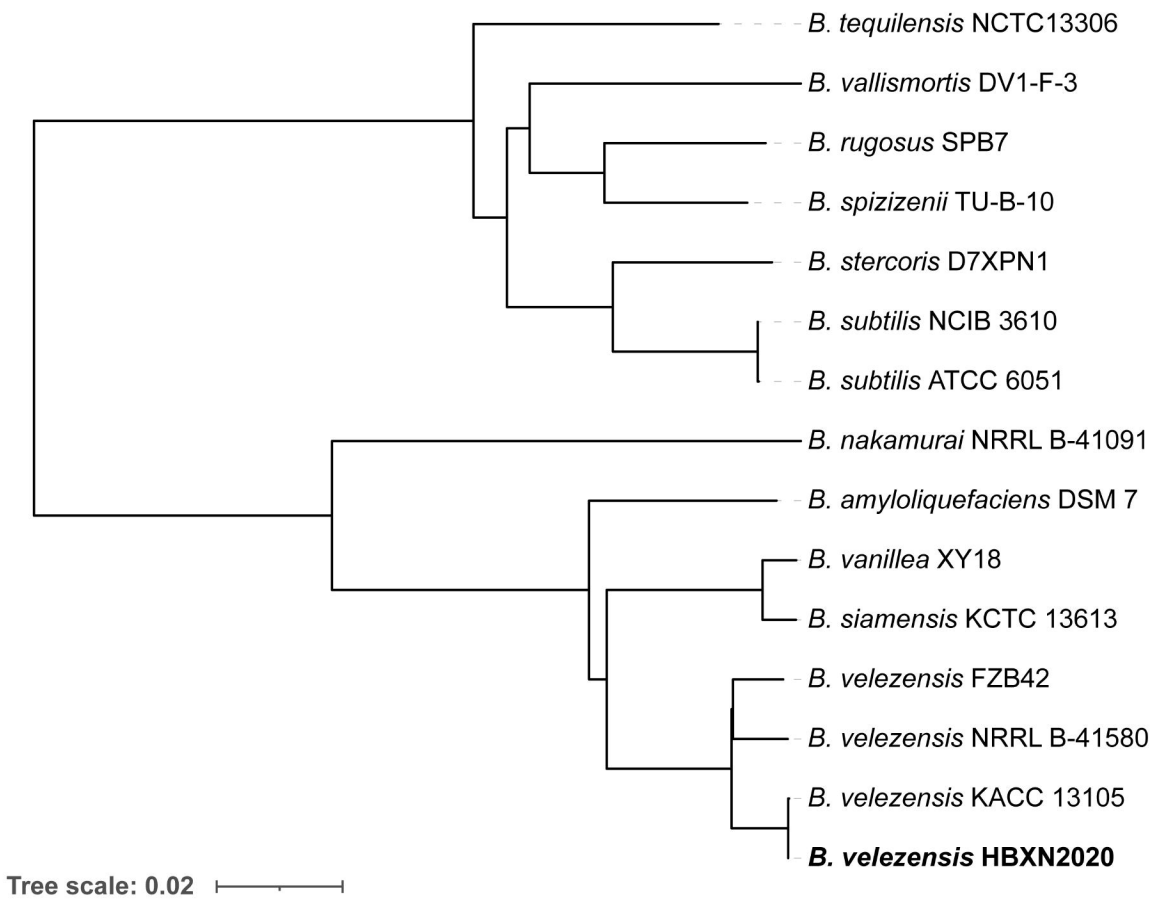
B. tequilensis NCTC13306
B. vallismortis DV1-F-3
B. rugosus SPB7
B. spizizenii TU-B-10
B. stercoris D7XPN1
B. subtilis NCIB 3610
B. subtilis ATCC 6051
B. nakamurai NRRL B-41091
B. amyloliquefaciens DSM 7
B. vanillea XY18
B. siamensis KCTC 13613
B. velezensis FZB42
B. velezensis NRRL B-41580
B. velezensis KACC 13105
B. velezensis HBXN2020
Tree scale: 0.02

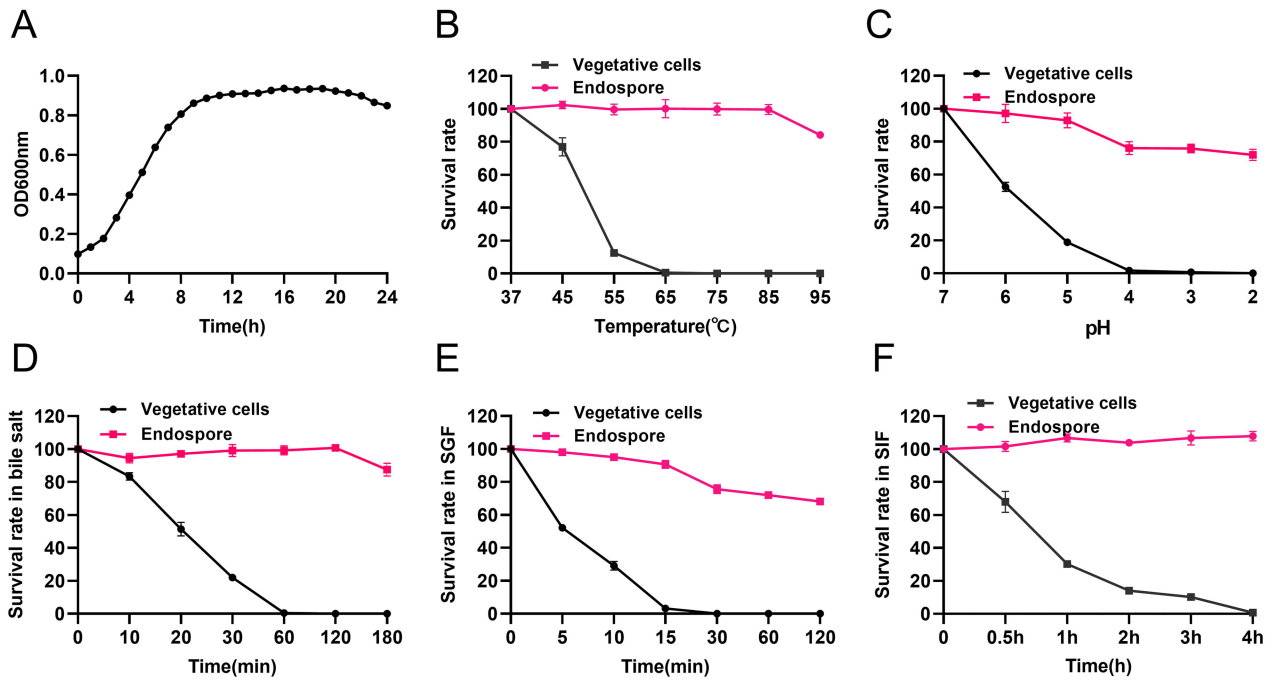
A
OD600nm
1.0
0.8
0.6
0.4
0.2
0.0
0
4
8
12
16
20
24
Time(h)
B
Vegetative cells
Endospore
Survival rate
120
100
80
60
40
20
0
37
45
55
65
75
85
95
Temperature(℃)
C
Vegetative cells
Endospore
Survival rate
120
100
80
60
40
20
0
7
6
5
4
3
2
pH
D
Vegetative cells
Endospore
Survival rate in bile salt
120
100
80
60
40
20
0
0
10
20
30
60
120
180
Time(min)
E
Vegetative cells
Endospore
Survival rate in SGF
120
100
80
60
40
20
0
0
5
10
15
30
60
120
Time(min)
F
Vegetative cells
Endospore
Survival rate in SIF
120
100
80
60
40
20
0
0
0.5h
1h
2h
3h
4h
Time(h)

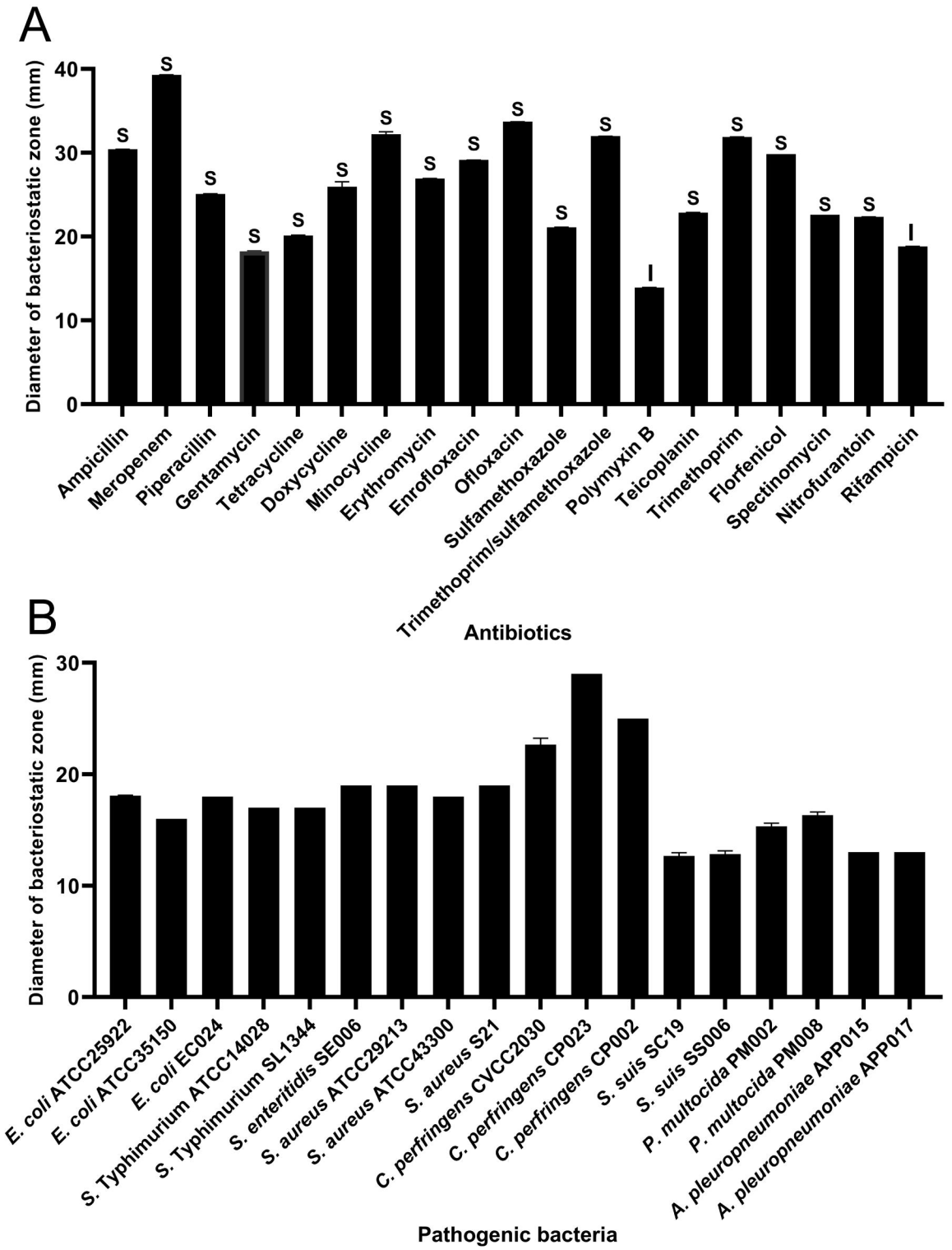
A
Diameter of bacteriostatic zone (mm)
0
10
20
30
40
S
S
S
S
S
S
S
S
S
S
S
I
S
S
S
S
S
I
Ampicillin
Meropenem
Piperacillin
Gentamycin
Tetracycline
Doxycycline
Minocycline
Erythromycin
Enrofloxacin
Ofloxacin
Sulfamethoxazole
Trimethoprim/sulfamethoxazole
Polymyxin B
Teicoplanin
Trimethoprim
Florfenicol
Spectinomycin
Nitrofurantoin
Rifampicin
Antibiotics
B
Diameter of bacteriostatic zone (mm)
0
10
20
30
E. coli ATCC25922
E. coli ATCC35150
E. coli EC024
S. Typhimurium ATCC14028
S. Typhimurium SL1344
S. enteritidis SE006
S. aureus ATCC29213
S. aureus ATCC43300
S. aureus S21
C. perfringens CVCC2030
C. perfringens CP023
C. perfringens CP002
S. suis SC19
S. suis SS006
P. multocida PM002
P. multocida PM008
A. pleuropneumoniae APP015
A. pleuropneumoniae APP017
Pathogenic bacteria

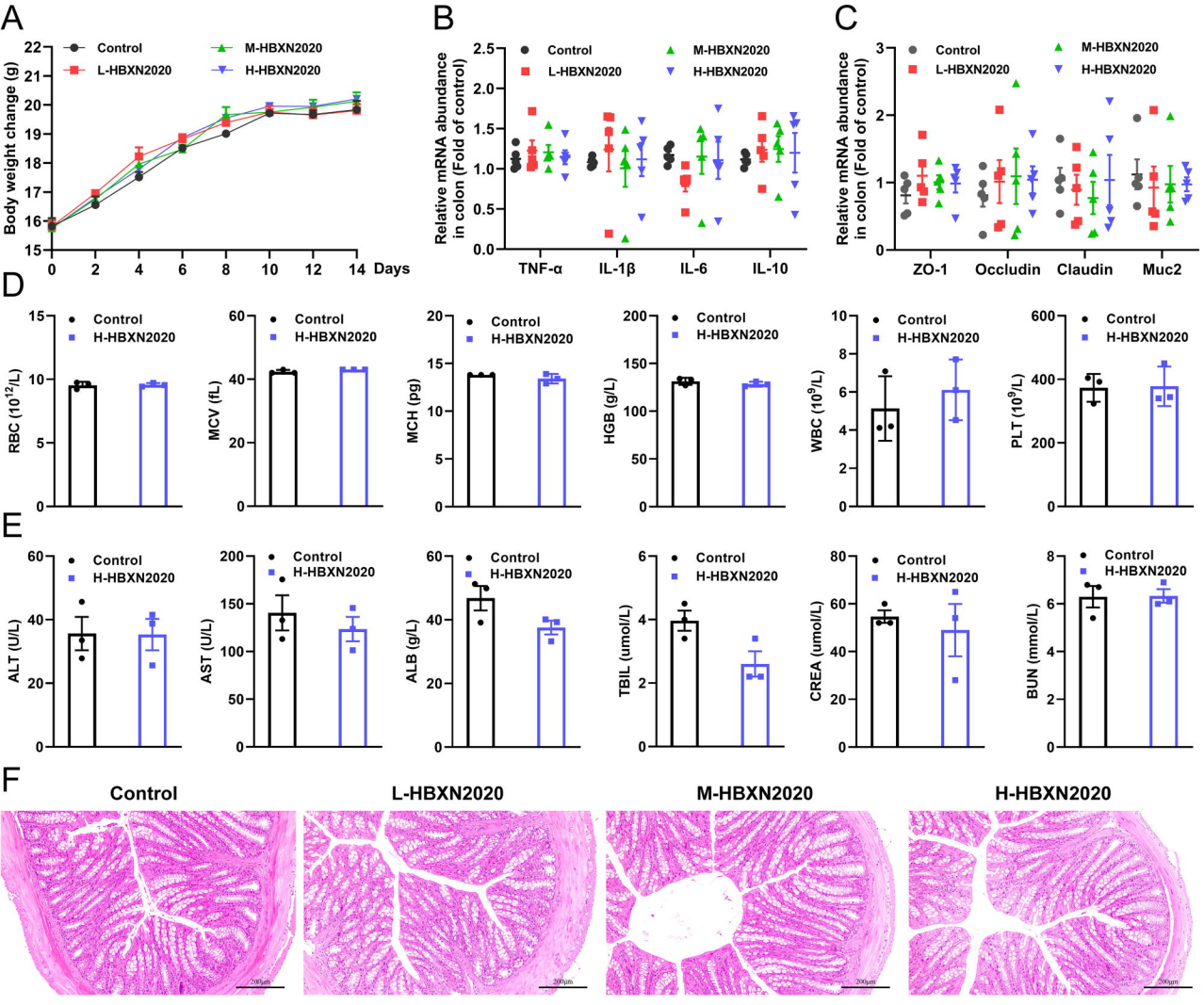
A
Control
L-HBXN2020
M-HBXN2020
H-HBXN2020
Body weight change (g)
Days
B
Relative mRNA abundance in colon (Fold of control)
TNF-α
IL-1β
IL-6
IL-10
C
ZO-1
Occludin
Claudin
Muc2
D
RBC (10^{12}/L)
MCV (fL)
MCH (pg)
HGB (g/L)
WBC (10^9/L)
PLT (10^9/L)
E
ALT (U/L)
AST (U/L)
ALB (g/L)
TBIL (umol/L)
CREA (umol/L)
BUN (mmol/L)
F
Control
L-HBXN2020
M-HBXN2020
H-HBXN2020

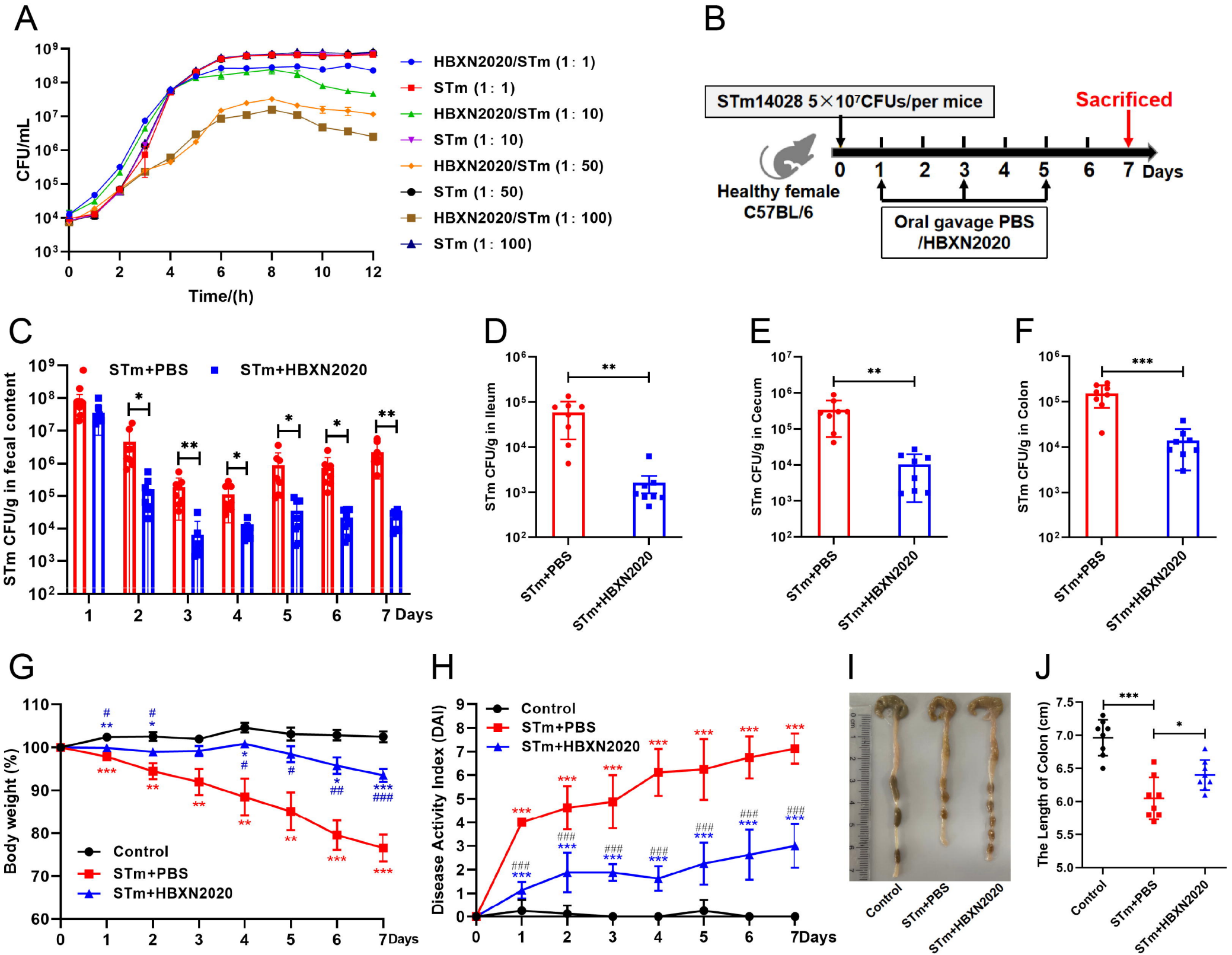
A
CFU/mL
Time/(h)
HBXN2020/STm (1：1)
STm (1：1)
HBXN2020/STm (1：10)
STm (1：10)
HBXN2020/STm (1：50)
STm (1：50)
HBXN2020/STm (1：100)
STm (1：100)
B
STm14028 5×10⁷CFUs/per mice
Sacrificed
Healthy female C57BL/6
Oral gavage PBS /HBXN2020
Days
C
STm+PBS
STm+HBXN2020
STm CFU/g in fecal content
Days
D
STm CFU/g in Ileum
E
STm CFU/g in Cecum
F
STm CFU/g in Colon
G
Body weight (%)
Control
STm+PBS
STm+HBXN2020
Days
H
Disease Activity Index (DAI)
Control
STm+PBS
STm+HBXN2020
Days
I
Control
STm+PBS
STm+HBXN2020
J
The Length of Colon (cm)
Control
STm+PBS
STm+HBXN2020

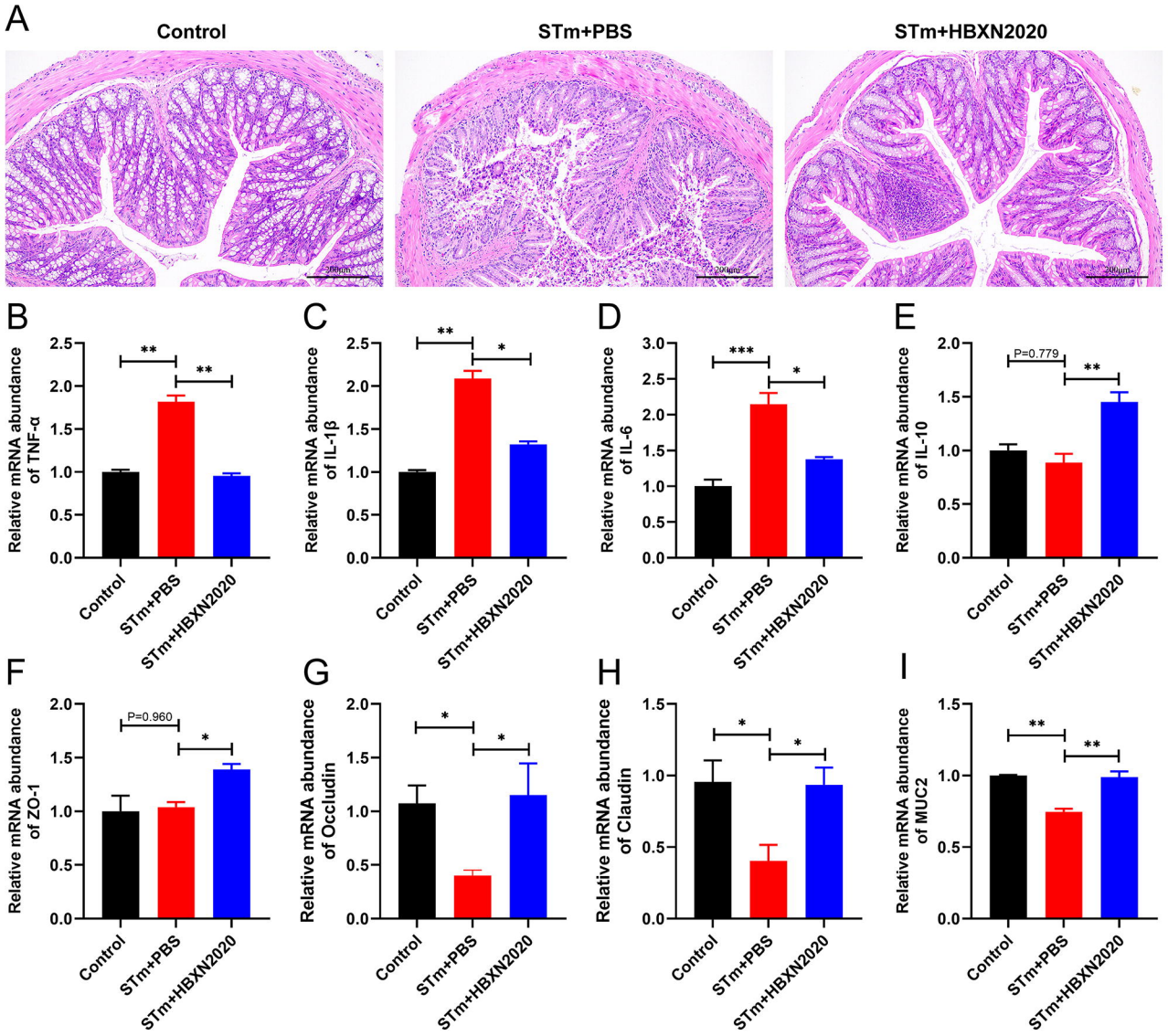
A
Control
STm+PBS
STm+HBXN2020
200μm
B
Relative mRNA abundance of TNF-α
C
Relative mRNA abundance of IL-1β
D
Relative mRNA abundance of IL-6
E
Relative mRNA abundance of IL-10
P=0.779
F
Relative mRNA abundance of ZO-1
P=0.960
G
Relative mRNA abundance of Occludin
H
Relative mRNA abundance of Claudin
I
Relative mRNA abundance of MUC2
Control
STm+PBS
STm+HBXN2020

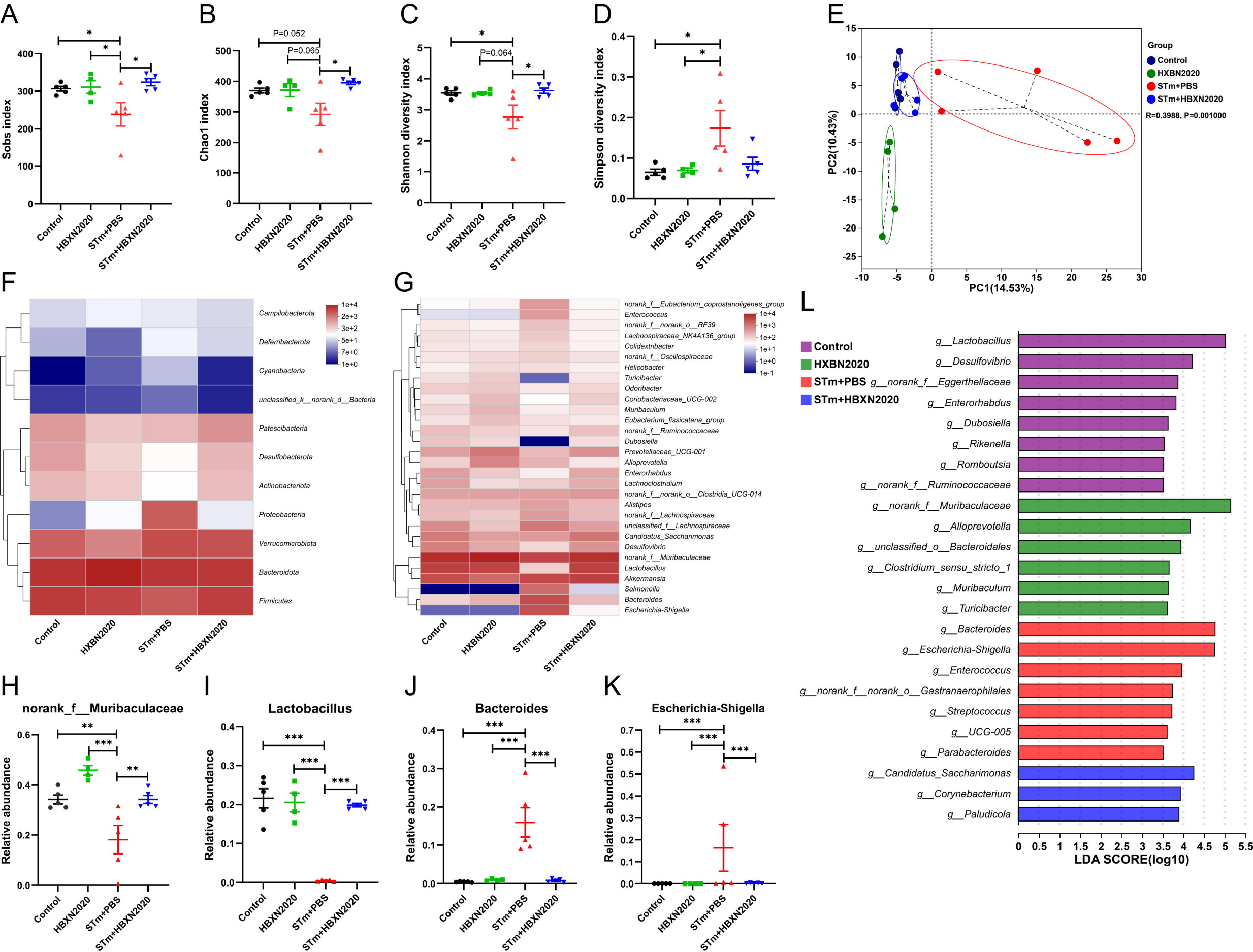
A
Sobs index
Control
HBXN2020
STm+PBS
STm+HBXN2020
B
Chao1 index
P=0.052
P=0.065
C
Shannon diversity index
P=0.064
D
Simpson diversity index
E
Group
Control
HXBN2020
STm+PBS
STm+HBXN2020
R=0.3988, P=0.001000
PC2(10.43%)
PC1(14.53%)
F
Campilobacterota
Deferribacterota
Cyanobacteria
unclassified_k__norank_d__Bacteria
Patescibacteria
Desulfobacterota
Actinobacteriota
Proteobacteria
Verrucomicrobiota
Bacteroidota
Firmicutes
G
norank_f__Eubacterium_coprostanoligenes_group
Enterococcus
norank_f__norank_o__RF39
Lachnospiraceae_NK4A136_group
Colidextribacter
norank_f__Oscillospiraceae
Helicobacter
Turicibacter
Odoribacter
Coriobacteriaceae_UCG-002
Muribaculum
Eubacterium_fissicatena_group
norank_f__Ruminococcaceae
Dubosiella
Prevotellaceae_UCG-001
Alloprevotella
Enterorhabdus
Lachnoclostridium
norank_f__norank_o__Clostridia_UCG-014
Alistipes
norank_f__Lachnospiraceae
unclassified_f__Lachnospiraceae
Candidatus_Saccharimonas
Desulfovibrio
norank_f__Muribaculaceae
Lactobacillus
Akkermansia
Salmonella
Bacteroides
Escherichia-Shigella
H
norank_f__Muribaculaceae
Relative abundance
I
Lactobacillus
J
Bacteroides
K
Escherichia-Shigella
L
Control
HXBN2020
STm+PBS
STm+HBXN2020
g__Lactobacillus
g__Desulfovibrio
g__norank_f__Eggerthellaceae
g__Enterorhabdus
g__Dubosiella
g__Rikenella
g__Romboutsia
g__norank_f__Ruminococcaceae
g__norank_f__Muribaculaceae
g__Alloprevotella
g__unclassified_o__Bacteroidales
g__Clostridium_sensu_stricto_1
g__Muribaculum
g__Turicibacter
g__Bacteroides
g__Escherichia-Shigella
g__Enterococcus
g__norank_f__norank_o__Gastranaerophilales
g__Streptococcus
g__UCG-005
g__Parabacteroides
g__Candidatus_Saccharimonas
g__Corynebacterium
g__Paludicola
LDA SCORE(log10)

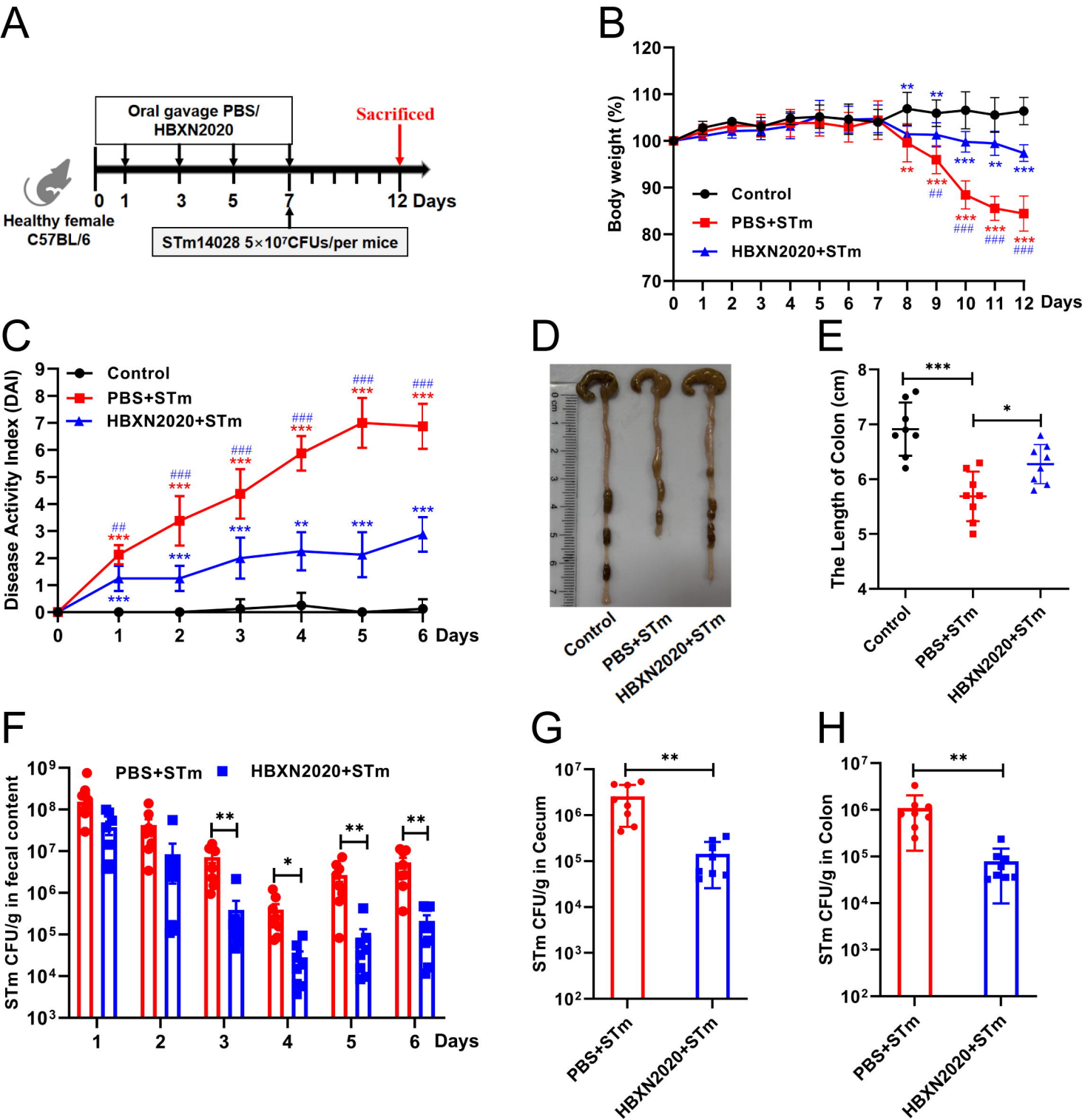
A
Oral gavage PBS/ HBXN2020
Sacrificed
Healthy female C57BL/6
0 1 3 5 7 12 Days
STm14028 5×10⁷CFUs/per mice
B
Body weight (%)
Control
PBS+STm
HBXN2020+STm
Days
C
Disease Activity Index (DAI)
Control
PBS+STm
HBXN2020+STm
Days
D
Control
PBS+STm
HBXN2020+STm
E
The Length of Colon (cm)
Control
PBS+STm
HBXN2020+STm
F
STm CFU/g in fecal content
PBS+STm
HBXN2020+STm
Days
G
STm CFU/g in Cecum
PBS+STm
HBXN2020+STm
H
STm CFU/g in Colon
PBS+STm
HBXN2020+STm

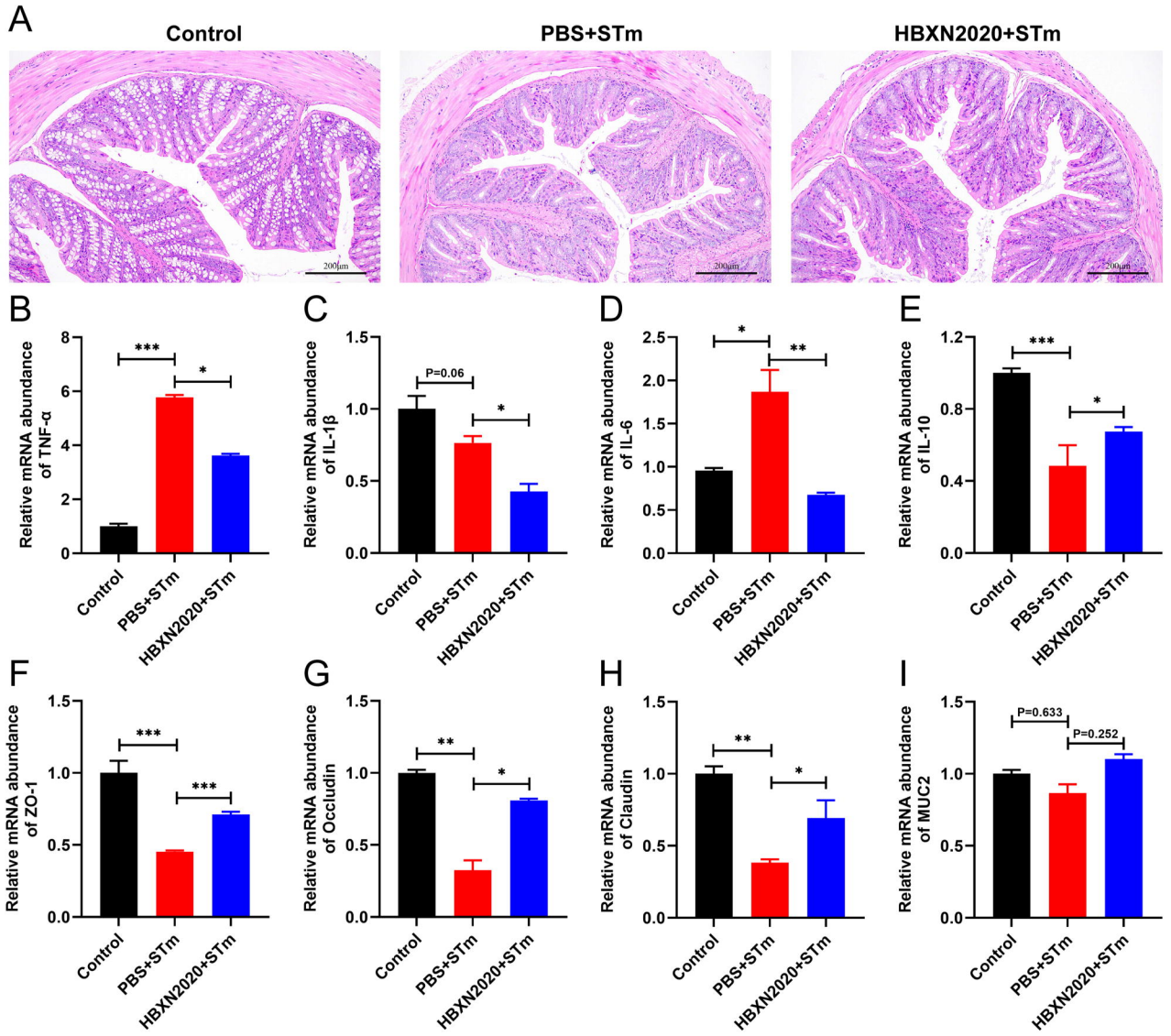
A
Control
PBS+STm
HBXN2020+STm
200μm
B
Relative mRNA abundance of TNF-α
C
Relative mRNA abundance of IL-1β
P=0.06
D
Relative mRNA abundance of IL-6
E
Relative mRNA abundance of IL-10
F
Relative mRNA abundance of ZO-1
G
Relative mRNA abundance of Occludin
H
Relative mRNA abundance of Claudin
I
Relative mRNA abundance of MUC2
P=0.633
P=0.252
Control
PBS+STm
HBXN2020+STm

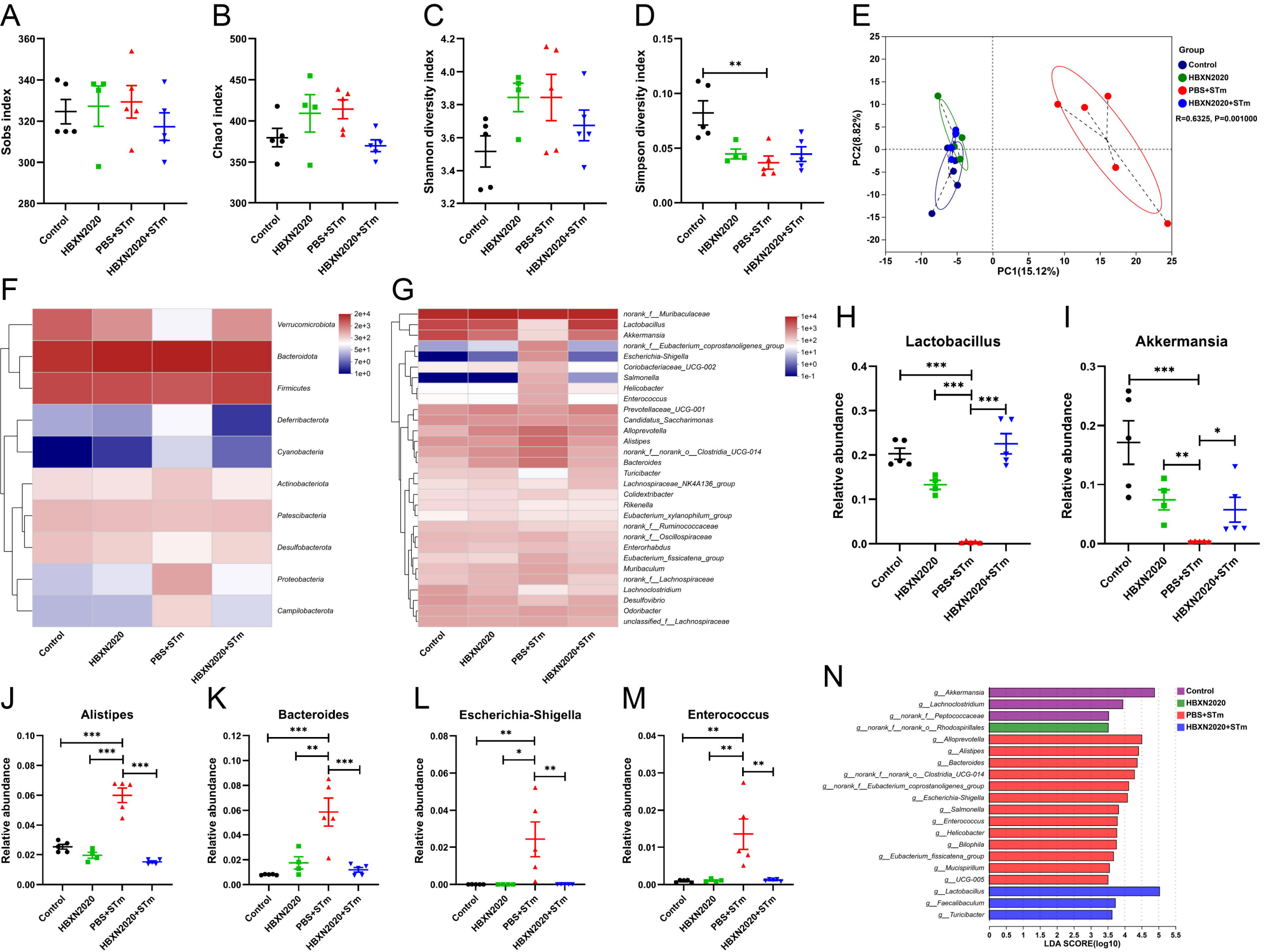
A
Sobs index
B
Chao1 index
C
Shannon diversity index
D
Simpson diversity index
**
Control
HBXN2020
PBS+STm
HBXN2020+STm
E
Group
Control
HBXN2020
PBS+STm
HBXN2020+STm
R=0.6325, P=0.001000
PC2(8.82%)
PC1(15.12%)
F
Verrucomicrobiota
Bacteroidota
Firmicutes
Deferribacterota
Cyanobacteria
Actinobacteriota
Patescibacteria
Desulfobacterota
Proteobacteria
Campilobacterota
G
norank_f__Muribaculaceae
Lactobacillus
Akkermansia
norank_f__Eubacterium_coprostanoligenes_group
Escherichia-Shigella
Coriobacteriaceae_UCG-002
Salmonella
Helicobacter
Enterococcus
Prevotellaceae_UCG-001
Candidatus_Saccharimonas
Alloprevotella
Alistipes
norank_f__norank_o__Clostridia_UCG-014
Bacteroides
Turicibacter
Lachnospiraceae_NK4A136_group
Colidextribacter
Rikenella
Eubacterium_xylanophilum_group
norank_f__Ruminococcaceae
norank_f__Oscillospiraceae
Enterorhabdus
Eubacterium_fissicatena_group
Muribaculum
norank_f__Lachnospiraceae
Lachnoclostridium
Desulfovibrio
Odoribacter
unclassified_f__Lachnospiraceae
H
Lactobacillus
I
Akkermansia
Relative abundance
J
Alistipes
K
Bacteroides
L
Escherichia-Shigella
M
Enterococcus
N
g__Akkermansia
g__Lachnoclostridium
g__norank_f__Peptococcaceae
g__norank_f__norank_o__Rhodospirillales
g__Alloprevotella
g__Alistipes
g__Bacteroides
g__norank_f__norank_o__Clostridia_UCG-014
g__norank_f__Eubacterium_coprostanoligenes_group
g__Escherichia-Shigella
g__Salmonella
g__Enterococcus
g__Helicobacter
g__Bilophila
g__Eubacterium_fissicatena_group
g__Mucispirillum
g__UCG-005
g__Lactobacillus
g__Faecalibaculum
g__Turicibacter
LDA SCORE(log10)